RUHR-UNIVERSITÄT BOCHUM
Fakultät für Geowissenschaften

Lehrstuhl für Geophysik Prof. Dr. H.-P. Harjes

Advanced Waveform Research Methods for GERESS Recordings

Semi-annual Report : 01 Jun 1993 - 30 Nov 1993

Air Force Geophysics Laboratory
Grant MDA 972-93-1-0022

Date : 15 December 1993

SECURITY CLASSIFICATION OF THIS PAGE

REPORT DOCUMENTATION PAGE

Form Approved
OMB No. 0704-0188

1a. REPORT SECURITY CLASSIFICATION	1b. RESTRICTIVE MARKINGS
2a. SECURITY CLASSIFICATION AUTHORITY	3. DISTRIBUTION/AVAILABILITY OF REPORT
2b. DECLASSIFICATION/DOWNGRADING SCHEDULE	
4. PERFORMING ORGANIZATION REPORT NUMBER(S)	5. MONITORING ORGANIZATION REPORT NUMBER(S)
6a. NAME OF PERFORMING ORGANIZATION: Ruhr-University-Bochum; 6b. OFFICE SYMBOL (If applicable): RUB	7a. NAME OF MONITORING ORGANIZATION
6c. ADDRESS (City, State, and ZIP Code): D-44780 Bochum, FEDERAL REPUBLIC OF GERMANY	7b. ADDRESS (City, State, and ZIP Code)
NAME OF FUNDING/SPONSORING ORGANIZATION: Advanced Research Projects Agency; 8b. OFFICE SYMBOL (If applicable): ARPA	9. [illegible] Grant No. : MDA 972-93-1-0022
8c. ADDRESS (City, State, and ZIP Code): 3701 North Fairfax Drive, Arlington, VA 22203-1714	10. SOURCE OF FUNDING NUMBERS: PROGRAM ELEMENT NO. / PROJECT NO. / TASK NO. / WORK UNIT ACCESSION NO.

11. TITLE (Include Security Classification)

Advanced Waveform Research Methods for GERESS Recordings

12. PERSONAL AUTHOR(S)
H.-P. Harjes, M. Jost, J. Schweitzer, G. Bokelmann

13a. TYPE OF REPORT	13b. TIME COVERED	14. DATE OF REPORT (Year, Month, Day)	15. PAGE COUNT
semiannual	FROM Jun/93 TO Nov/93	1993-12-15	

16. SUPPLEMENTARY NOTATION

17. COSATI CODES			18. SUBJECT TERMS (Continue on reverse if necessary and identify by block number)
FIELD	GROUP	SUB-GROUP	Arrays, Calibration, Regional Wave Propagation GERESS

19. ABSTRACT (Continue on reverse if necessary and identify by block number)

The German Experimental Seismic System (GERESS) is operated by Ruhr-University Bochum, Germany. It is an extension of the Scandinavian regional array network, i.e. NORESS, ARCESS, and FINESA, into Central Europe. This report summarizes research activities carried out at the data centre in the Institute of Geophysics in Bochum during the first semiannual period (June - November 1993) of the current grant. GERESS data are continuously transmitted from the array hub in Bavaria to Bochum and analyzed by an on-line processing system, based on RONAPP, to locate seismic events in near real-time. In 1993, Ruhr-University continued the on-site maintenance of the array as part of the research grant. As described in detail in the status report (M. Jost), the monthly uptime of the array varied during the reporting period between 99.3 % and 88.6 % with an average of 97.4 % .

Two major research projects were finished and separated papers are included in this report. The first report (J. Schweitzer) explores specific path effects for regional waves in Central Europe. Data from the Group of Scientific Experts' Second Technical Test (GSETT-2) clearly show the influence of an ancient border line between the East European Platform and the

(continued)

20. DISTRIBUTION/AVAILABILITY OF ABSTRACT	21. ABSTRACT SECURITY CLASSIFICATION	
☐ UNCLASSIFIED/UNLIMITED ☐ SAME AS RPT. ☐ DTIC USERS		
22a. NAME OF RESPONSIBLE INDIVIDUAL	22b. TELEPHONE (Include Area Code)	22c. OFFICE SYMBOL

West European Orogen which is known as the Teisseyre-Tornquist zone (TTZ). The TTZ seems to squelch seismic waves, thereby increasing the detection threshold for stations on the opposite side by at least one magnitude unit. To explain these observations, the wave propagation of Pn and Pg, crossing the TTZ perpendicularly, was modeled with Gaussian beam seismograms. To defocus or damp the seismic energy, the TTZ as a structural anomaly between Eastern and Western Europe must reach down into the upper mantle to a depth of at least about 200 km.

The second report (G. Bokelmann) addresses the problem of array calibration with respect to azimuth and slowness. The GSE is currently developing a final concept for an international seismic data exchange system which includes a two-tiered global network of stations where the first tier, the so-called alpha-network, consists primarily of arrays and is designed to provide not only the required detection threshold throughout the world but also to achieve a preliminary event location. It is therefore of utmost importance that the alpha arrays which include GERESS are carefully calibrated. Determination of mislocation vectors is an essential part of this calibration. After careful reading of onset times at GERESS, slowness uncertainties were reduced to about 0.5 s/degree, while azimuthal uncertainties were about 2 degrees for regional events and less than 5 degrees for teleseismic events under favorable snr-conditions. The precise determination of the slowness vector, however, requires array topography (about 200 meters for GERESS) to be taken into account. Such a 3D array allows determination of the vertical slowness, which gives a reasonable local velocity of 5.2 km/s under the GERESS array.

TABLE OF CONTENTS

1. GERESS STATUS REPORT

January 1993 - November 1993

Michael L. Jost

1.1 General

The German Experimental Seismic System (GERESS) is operated by Ruhr-University Bochum, Germany. It is an extension of the Scandinavian regional array network, i. e., NORESS, ARCESS, and FINESA, into Central Europe. The GERESS array is located in the Bavarian Forest area at the southeastern part of Germany near the border to Austria and Czechoslovakia. The array consists of 25 stations with vertical-component short-period Teledyne Geotech GS-13 instruments sampled at 40 Hz. In addition, four of the sites include horizontal component instruments. At the key station of the array, GEC2 (48.84511 N, 13.70156 E, 1132 m), a STS-2 is sampled with 80 Hz (broad-band element). The geometry of the array is based on concentric rings providing an overall aperture of about 4 km. The GERESS aperture is larger than that of NORESS by a factor of 4/3 which resulted from signal and noise correlation measurements by Harjes (1990). The array became fully operational in January 1991. Data from the array are continuously transmitted to the NORSAR data center in Kjeller and to the Institute of Geophysics, Ruhr-University Bochum via 64-kbit lines.

This report summarizes the technical performance of GERESS and continues similar descriptions given previously (Jost, 1991a; 1992a; 1993). This summary is based on monthly status reports that are available upon request.

1.2 GERESS Observatory at Ruhr-University Bochum

The Department of Geophysics of Ruhr-University Bochum operates an experimental on-line processing system for GERESS data (Jost 1992b; Harjes et al., 1993b). This system uses software developed at NORSAR (Mykkeltveit and Bungum, 1984; Fyen, 1987). The automatic analysis has worked very stable and results of the analysis are available for 100 % of the available GERESS data from Jan. - Nov. 1993.

The on-line processing consists of 3 steps: detection, fk-analysis, and location. The first stage of the on-line processing accesses data in 30 second

segments and runs a STA/LTA detector. The detector presently recognizes an onset if the STA/LTA ratio for a filtered trial-beam exceeds a threshold of 4. Since September 1993, horizontal beams have been included to improve on S-type detections. The next step of the on-line processing is the transformation of a 3 second filtered data segment at each onset time (derived from the detection time) into the frequency-wavenumber domain. As a result, the slowness and back-azimuth of the phase is determined. From the slowness information, seismic phases are identified. The final step of the on-line data processing is the location of events. The seismic phases as identified in the fk-analysis are associated to events in this step. From the arrival time difference of regional phases, the distance to the epicenter can be determined from the Jeffreys - Bullen travel time tables for regional seismic phases. Together with a mean back-azimuth, the epicenter locations of local and regional events are determined. Correcting for outages, 20 events have been automatically located each day on average (Table 1-1). Figure 1-1 shows the automatic event locations for Jan. - Nov. 1993. Local magnitudes automatically determined at Bochum (e. g. Jost, 1993) appear low by at least 0.5 magnitude units compared to values published by other European networks. A new algorithm will be implemented shortly.

Alert messages for strong teleseismic and regional events are automatically sent to NEIC (Golden, CO) and other interested institutions in near real-time. 75 times, a GERESS alert message for a teleseismic onset has been used in the NEIC alerts from Jan.-Nov. 1993. For regional events, a fast earthquake information system (FEIS) has been developed (Schweitzer, Schulte-Theis, Jost) and operated at Bochum. Starting from a GERESS automatic detection above a certain threshold, the routine automatically accesses the detection logs of the German Regional Seismic Network (GRSN). Using all available detections from this network, the routine proceeds to calculate a new location which is subsequently e-mailed to interested institutions. The time difference between origin time and transmission of an alert message was 42 minutes for more than 84 % of all FEIS alerts (Jul 93 - Oct 93). The shortest time was 24 minutes, the longest 1 hour.

At Bochum, analysts reviewed interesting regional events. They repicked onset times, redetermined back-azimuths and phase velocities, and relocated events using the LOCSAT routine which is a modified version of TTAZLOC (Bratt and Bache, 1988). From Jan.-Nov. 1993, 2217 regional phases have been reviewed and 896 regional events have been relocated (Figure 1-2). In addition, teleseismic events have been routinely reevaluated by an analyst, and parameter data (onset time, amplitude, period, azimuth, and slowness) for 14684 phases (i.e., 44 phases per day) have been sent to NEIC (Golden, CO), ISC, and other institutions from Jan.-Nov. 1993.

In the following, 2 interesting teleseismic events are shown. On Sep. 22, 1993, 07:01:080, the non-proliferation experiment (NPE) was detonated on the Nevada test site (tunnel under Ranier Mesa). The yield was reported as about 1.0 kT (Denny and Zucca, 1993). The coordinates are 37.202 N and 116.210 W, h= 390 m, elev=1852.5 m. The GERESS data center in Bochum automatically detected its P-wave at 07:13:29.6 with a SNR of 5.4 at an epicentral

distance of 83.5 deg. The analyst reviewed parameters are 07:13:29.2, T=0.97 sec, A=1.34 nm, slo=5.73 sec/deg, baz=335 deg yielding a mb(GERESS) = 4.04. Figure 1-3 shows the beam trace (1-3 Hz, 5.13 sec/deg, 322 deg) on top and the key station C2 on bottom.

The second example shows the GERESS record of the Oct 5, 1993 presumed nuclear test at the Chinese test site Lop Nor (01:59:56.58 41.647N 88.681E mb=5.9; from PDE weekly). The GERESS data center in Bochum automatically detected its P-wave at 02.09.04.7 with a SNR of 118 at an epicentral distance of 51.3 deg. The analyst reviewed parameters are 02:09:04.7, T=1.13 sec, A=24.88 nm, slo=7.67 sec/deg, baz=64 deg yielding a mb(GERESS) = 5.3. Figure 1-4 shows the beam trace (unfiltered, 7.50 sec/deg, 68 deg) on top and the key station C2 on bottom. Note the PcP onset at 02:10:20.0.

GERESS is an open station and results of the on-line processing have been sent to interested institutions via e-mail (e.g. Bundesanstalt für Geowissenschaften und Rohstoffe (BGR), EMSC, Frankfurt University, Gräfenberg Array, ING, KTB array, LDG, Leipzig University, Stuttgart University, NORSAR, Oklahoma Geol. Survey, ORFEUS, and seismological institutes in Austria, CZ, Hungary, Slovenija, Switzerland; YKA). In addition, the On-line Processing Display Manager (Jost, 1991b) has been used by many scientists for near real time information on parameter data. The Data Request Manager (DRM) by Krake Inc. is operated in trial mode. The DRM should enable the transmission of data (GSE, SEED) and interfaces to the German Regional Network of Broad-Band Stations.

Table 1-1
Statistics on the GERESS Bochum On-line Processing for Jan.-Nov. 1993

	number	number/day
detections	72993	225
f-k analyses	61816	190
locations	6444	20

In early 1993, the data acquisition software (TM Science Horizons) was again upgraded and became sufficiently robust. Now, the MTBF of the data acquisition software is about 5 months. The upgrade addressed the problems of software crashes (MRG) and corrupted time stamps of the RDAS-200.

1.3 GERESS Array Hub

The GERESS array showed stable operation from Jan. - Nov. 1993. Table 1-2 shows the uptime of the system including the Bochum Observatory (uptimes directly correspond to the data archived in Bochum). The average uptime was 97.4 %, i.e., the total outage amounts to 8 days 18 hours. The highest uptime (99.3 %) was observed in March 1993; the lowest uptime (88.6 %) occurred in July 1993 due to thunderstorm damage at the array site. Table 1-3 further specifies the causes of the observed outages. The technical status of GERESS is summarized in chronological order in Appendix 1-1. Results of a recent instrument calibration are given in Appendix 1-2. In regular operation, we loose about 1.3 sec of data for each channel and day which may be attributed to IAC, Telekom data line, and data acquisition hard- (SHI's white box) and software (SHI's SAVE).

The technical installation of GERESS had been classified "not fully acceptable" based on findings during the GERESS System Verification Test in September 1991 (Golden et al., 1991). The remaining problem was the repeated data dropouts of the Intelseis Array Controller (IAC). These dropouts ("9-second data gaps") were characterized by a stop of data transmission on all channels that are connected to a specific DigiBoard (TM). The data outage was in the order of about 9 seconds. Based on my observation that repeated data preceded each data dropout, John Poetschke of Teledyne-Geotech developed some monitoring software. He came to the GERESS hub from Jul 24 - Aug 7 to analyze this problem. He found that the data dropouts were caused by a hardware related problem of page faulting in the shared memory section of the

Table 1-2
GERESS uptime Jan.-Nov. 1993 (incl. Bochum data center)

Month	uptime %
Jan	99.1
Feb	96.3
Mar	99.3
Apr	98.3
May	96.3
Jun	98.0
Jul	88.6
Aug	98.9
Sep	98.8
Oct	98.9
Nov	98.7

Table 1-3
Causes of GERESS downtimes Jan.-Nov. 1993 (incl. Bochum data center)
(The total downtime was 757053 sec = 8d 18h 17m 33 sec)

cause	downtime [sec]	downtime [%]
Bochum data acq. software	147764	19.5
Bochum data acq. software (maintenance)	4652	0.6
Bochum data acq. workstation	16271	2.2
Bochum CIM	30	0.0
Bochum power outage	7866	1.0
total outage Bochum	176583	23.3
Communication line	148294	19.6
HUB IAC crashes (8)	95974	12.7
HUB thunderstorm damage	219741	29.0
HUB maintenance	92274	12.2
HUB power outage	3695	0.5
total outage HUB	411684	54.4
other causes	20492	2.7

DigiBoard. The mean probability of a bad page change (of the shared memory) was 1/700 - 1/2200 (DigiBoard 2 - DigiBoard 4, respectively). Based on this result, J. Poetschke found a work-around (minimizing page faulting) which completely eliminated this problem. During his visits he also fixed an old bug: Now, each station will synchronize with the GERESS master clock after it comes on-line after a power shutdown. On the other hand, the MTBF of the IAC has remained at a low level of about 2 weeks.

Unfortunately, Teledyne-Geotech discontinued seismological data acquisition systems (i.e. RDAS-200, IAC). Obviously, its inherent problems will never be solved, that's why I give a final list here (these problems are well known and documented e.g. 1990-, 1991-, 1992-, 1993 GERESS Status Reports):

- The RDAS-200 occasionally sends data with corrupted time stamps in the future.

- The RDAS-200 occasionally sends electronic noise instead of seismic data after power up or self-reset (Figure 1-5). This state can be cleared only by manual intervention (reset).

- If the 1pps timing-signal is bad (optical modems, fiber optic link) or the clock-board in the RDAS-200 deteriorates before completely failing, data are desynchronized by less than a second. Only an array has the chance to

detect this (Figure 1-6). Each day, a careful inspection of the records is required to insure proper synchronization.

- The RDAS-200 is very sensitive to spikes in input voltage (thunderstorms).

- Meteorological data are not available for GERESS.

- The GPS receiver purchased for GERESS has neither been delivered nor implemented as planned - GERESS runs on DCF-77.

- The UPS can bridge a power outage of only 10 minutes in duration.

- Data compression has not been implemented. This causes extensive communication costs. The full SDLC protocol is not realized - data dropouts due to communication line problems can result.

At Bochum data center, we have continued to keep GERESS up and running to provide the research community with excellent data. We hope that we will obtain sufficient spare parts to keep the current hardware running as long as practical. For a treaty situation, an upgrade of the present hardware to a significantly more robust system is strongly suggested.

In Feb. 1993, the data link GERESS - Kjeller was modified. The reason was that Teledyne's second "independent" data line out of the GERESS IAC has never really worked properly (GERESS Status Reports). The performance of this data link has not even been tested during the GERESS systems acceptance test at the end of 1991 (Golden et al. 1991). The data center at Kjeller had been provided with GERESS data that showed at least a factor of 10 higher data gap rate than at Bochum. The data link to Kjeller showed a significant deterioration in fall of 1992: the data center at Kjeller did not receive any seismologically usable data. The telephone companies had checked the data line many times to find them within specs each time. However, Teledyne-Geotech did not help in isolating the problem. At that point, the data centers at Kjeller and Bochum decided to establish a WAN between both data centers. The second data line out of the GERESS array-controller was terminated. Our colleagues at Kjeller data center developed and installed a software that enabled the on-line transmission of GERESS data from Bochum.

1.4 Conclusion

GERESS is the most sensitive seismological station in Central Europe (e. g., Harjes et al., 1993a). The detection threshold of GERESS is below 1 kT for the Nevada test site (this report) as well as for the test site in the Tuamotu archipelago (Schweitzer et al., 1992).

At the GERESS data center Bochum, the observatory routine has included data archival and automatic on-line analysis. From Jan. to Nov. 1993, 20

regional events have been automatically located each day on average. The automatic locations of regional events render a good first solution, in general. The GERESS data center Bochum is the only German station that provides NEIC and interested institutions with alert messages (teleseismic and regional (FEIS)).

In Bochum, 896 regional events were relocated by analysts during the reporting time. In addition, extensive parameter data for 44 teleseismic phases have been interactively determined each day on average. Results of the interactive re-analysis of GERESS data have been used by NEIC, ISC, and other interested institutions. The Bochum observatory is an open station similar to the German Regional Network of Broad-Band Stations. In addition, Bochum serves as data center where various bulletins (e.g., automatic NEIC locations, NEIC alerts, QED, PDE (weekly), PDE (monthly), fast CMT's from Harvard, IMS locations, LDG locations, ING locations, Swiss alerts, Swiss bulletins (SED), Czech bulletins, and onset lists of YKA) are available for the interested user.

The GERESS data center Bochum has helped the CSS to test the experimental GSETT-3 International Data Center (IDC V0, since May 1993). Within this concept, GERESS served as α-station and acted as a node to access data from the GRSN, serving as β-stations.

The GERESS data center Bochum has been responsible for GERESS maintenance. The average GERESS uptime which includes the Bochum observatory has increased to 97.4 % from Jan. - Nov. 1993. This uptime is 0.5 % higher than in 1992 which again demonstrates the high level of reliability of the installation, its successful maintenance, and the high motivation of key personnel who substituted dedication for bad engineering.

Acknowledgements

J. Schweitzer and N. Schnieders supported the daily observatory routine. B. Klotz and L. Kühne conducted the maintenance work at the array site. Yan Jia, O. Mindavalli, and H. Schulte-Theis relocated regional events. J. Schweitzer and M. Jost reviewed teleseismic onsets. The communication software transmitting GERESS data to Kjeller (WAN) had been developed and installed by R. Paulsen (NORSAR). The help by Jan Fyen (NORSAR) in upgrading the data analysis software package is greatly appreciated. Special thanks are expressed to J. Poetschke (Teledyne-Geotech) for his effort to fix the "9-second" data gaps. The help of IRIS sending RDAS-200 spare parts is greatly acknowledged. The GERESS array has been funded by ARPA and its operation has been supported by grant MDA972-93-1-0022.

Literature

Bratt, S. R. and T. C. Bache (1988). Locating events with a sparse network of regional arrays, *Bull. Seism. Soc. Am.* **78,** 780-798.

Denny, M. and J. Zucca (1993). DOE non-proliferation experiment includes seismic data, *EOS, Trans. Am. Geophys. Un.* **74,** No. 45, 527.

Fyen, J. (1987). Improvements and Modifications, Semiannual Technical Summary, 1 October 1986 - 31 March 1987, *NORSAR Sci. Rep. No. 2-86/87*, Kjeller, Norway.

Golden, P., E. T. Herrin, and C. Hayward (1991). Development of an intelligent seismic facility and preparation for participation in the conference on disarmament group of scientific experts technical test. Results of the GERESS verification test, *Quarterly Technical Report SMU-R-91-152*, Southern Methodist University, Dallas, Texas, 64 pp.

Harjes, H.-P. (1990). Design and siting of a new regional array in Central Europe, *Bull. Seism. Soc. Am.* **80,** 1801-1817.

Harjes, H.-P., M. L. Jost, and J. Schweitzer (1993a). GERESS - a key station in a future global monitoring network, in Lewkowicz, J. F. and J. M. McPhetres (eds.) *Proceedings of the 15th annual seismic research symposium 8-10 September 1993* 139-145.

Harjes, H.-P., M. L. Jost, J. Schweitzer, and N. Gestermann (1993b). Automatic seismogram analysis at GERESS, *Computers & Geosciences* **19,** 157-166.

Jost, M. L. (1991a). GERESS status report January 1990 - March 1991, in *Advanced Waveform Research Methods for GERESS Recordings*, DARPA Annual Report No. AFOSR-90-0189, 28-37.

Jost, M. L. (1991b). The Bochum on-line processing display manager, in *Advanced Waveform Research Methods for GERESS Recordings*, DARPA Annual Report No. AFOSR-90-0189, 38-43.

Jost, M. L. (1992a). GERESS status report April 1991 - February 1992, in *Advanced Waveform Research Methods for GERESS Recordings*, DARPA Annual Report No. PL-TR-92-2142, 1-12.

Jost, M. L. (1992b). Current status and results of the GERESS data center in Bochum, in *Proceedings of the GERESS Symposium Waldkirchen June 22-24, 1992*, 93-102.

Jost, M. L. (1993). GERESS status report January 1992 - December 1992, in *Advanced Waveform Research Methods for GERESS Recordings*, ARPA Annual Report No. PL-TR-93-2172, 1-17.

Mykkeltveit, S. and H. Bungum (1984). Processing of regional seismic events using data from small-aperture arrays, *Bull. Seism. Soc. Am.* **74,** 2313-2333.

Schweitzer, J., M. L. Jost, N. Gestermann (1992). Nuclear tests observed with the GERESS array in 1991, in *Advanced Waveform Research Methods for GERESS Recordings*, DARPA Annual Report No. PL-TR-92-2142, 50-59.

Wüster, J. (1993). Report on GERESS instrument calibration, in *Advanced Waveform Research Methods for GERESS Recordings*, ARPA Annual

Report No. PL-TR-93-2172, 18-32.

Appendix 1-1: Chronological Status List GERESS

Jan. 1993:
- power outage HUB (repair work by electricity company)
- power outage Bochum (repair work at university)
- IAC crashes: 2
- malfunctions of data acquisition software documented
- Jan. 1 - 2, maintenance visit at HUB.
- termination of data line HUB - NORSAR data center

Feb. 1993:
- WAN between Bochum and NORSAR data centers established
- upgrade of SHI's (v. 8.2.1) data acquisition software implemented
- pager installed to notify manager on duty of fatal system crashes

Mar. 1993:
- Mar 3 - 7, Mar 29 - Apr 2 maintenance visits at HUB (board level repair of IAC multifunction module to fix clock interface).
- synchronous crashes of various RDAS appeared due to defective DC/DC converters in vaults
- documenting new evidence (data retransmissions) on "9-second" data gap problem of the IAC
- D7 desynchronized by fraction of second due to defective optical modem

Apr. 1993:
- synchronous crashes of various RDAS due to defective DC/DC converters in vaults
- Apr 14 - 23 maintenance visit by RUB engineers.

May 1993:
- synchronous crashes of various RDAS due to defective DC/DC converters in vaults
- May 4-7 and 25 - 28: maintenance visit by RUB engineers
- 5 times thunderstorm damage (outages of channels and destruction of data modem)
- D7 desynchronized by fraction of second due to defective clock module

Jun. 1993:
- IAC crashes: 2
- 6 times thunderstorm damage (outages of channels)
- installation of modem based power cycling equipment at HUB
- June 21 - Jul 2: maintenance visit by RUB engineers

- test software by Teledyne-Geotech: the "9-second" data gaps are not caused by software induced resets of the DigiBoards in the IAC.
- D5 desynchronized by fraction of second due to defective clock module
- upgrade of data request manager (DRM, Krake Inc)

Jul. 1993:

- 10 times thunderstorm damage (outages of channels and destruction of data modem converter)
- Jul 19 - 20, Jul 24 - Aug 8 maintenance visit by RUB engineers.
- Warranty repair work by Teledyne-Geotech at HUB to identify the cause of the "9-second" data gap problem. The cause of the data dropouts were located in the shared memory administration due to occasional hardware failure of the Digi-Boards.
- D5 desynchronized by fraction of second due to defective clock module
- Visit of Jan Fyen (NORSAR data center) and upgrade of data analysis software package
- development of FEIS (Fast Earthquake Information System) at Bochum: fast locations of regional events using GERESS and GRSN

Aug. 1993:

- 10 times thunderstorm damage (outages of channels)
- IAC crashes: 2
- Aug 31 - Sep 8: maintenance visit by RUB engineers

Sep. 1993:

- Warranty repair work by Teledyne Geotech: New software on DigiBoards (eproms) and IAC completely fixed the "9-second" data gap problem
- D2 desynchronized by fraction of second due to defective clock module (station suspended due to missing spare parts)
- new detector recipe using horizontal channels for S-type waves

Oct. 1993:

- IAC crashes: 3

Nov. 1993:

- Nov 16-21 and 25-28, maintenance work at HUB, installation and tests of satellite transmission equipment
- D2 up after exchange of clock module (provided by IRIS)

Appendix 1-2: GERESS Instrument Calibration

Each day, the GS-13's of GERESS are calibrated using a 1 Hz sinusoidal input voltage (GS-13 4500 mV, BB-13 1000 mV) fed to the calibration coil.

cal. time	channel
3:00 - 3:00:50	A0, A-ring (verticals), C2-sz
3:00 - 3:01:00	D6
3:01 - 3:01:50	A2-sn
3:02 - 3:02:50	A2-se, B - ring
3:04 - 3:04:50	C1, C3
3:06 - 3:06:50	D1-sz, D2, D3
3:07 - 3:07:50	D1-sn, D4-sn, D7-sn
3:08 - 3:08:50	D1-se, D4-se, D7-se, C4, C5, C6, C7
3:10 - 3:10:50	D4-sz, D5
3:12 - 3:12:50	D7-sz, D8, D9

Calibration on Nov 29, 1993 (318273 cnts are expected; Wüster, 1993)

channel	cnt	deviation in %
GEA0-sz	316602	-0.525
GEA1-sz	319789	0.476
GEA2-sz	311406	-2.16
GEA3-sz	316789	-0.466
GEB1-sz	319698	0.488
GEB2-sz	317055	-0.383
GEB3-sz	4369790	waveform ok
GEB4-sz	320854	0.811
GEB5-sz	307710	-3.32
GEC1-sz	314663	-1.13
GEC2-sz	312856	-1.70
GEC3-sz	315465	-0.882
GEC4-sz	312329	-1.87
GEC5-sz	312619	-1.78
GEC6-sz	315823	-0.770
GEC7-sz	426438	waveform ok
GED1-sz	294319	-7.53
GED2-sz	324797	2.05
GED3-sz	319470	0.376
GED4-sz	302276	-5.03
GED5-sz	313228	-1.59
GED6-sz	318432	0.050
GED7-sz	1216	currently not calibrated
GED8-sz	2771850	waveform ok
GED9-sz	1531	waveform too small
GEA2-sn	319073	0.251
GEA2-se	316167	-0.662
GED1-sn	323911	1.77
GED1-se	314829	-1.08
GED4-sn	313230	-1.58
GED4-se	313811	-1.40
GED7-sn	825	currently not calibrated
GED7-se	864	currently not calibrated
GEC2-hn	9297	currently not calibrated
GEC2-hz	11884	currently not calibrated
GEC2-he	9926	currently not calibrated

Figure 1-1:

GERESS Bochum: Automatic Locations Jan-Nov 1993

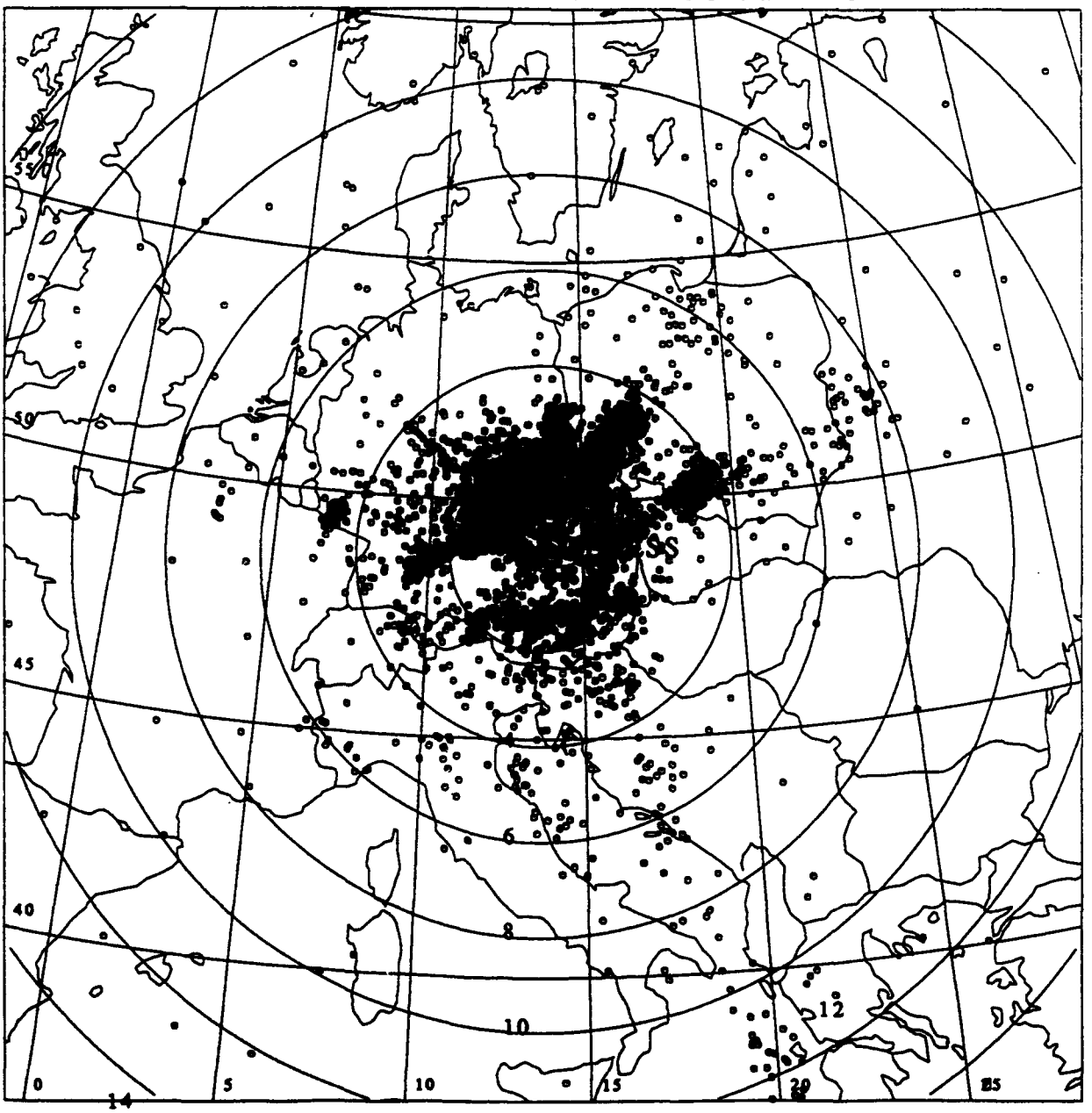

Figure 1-2:

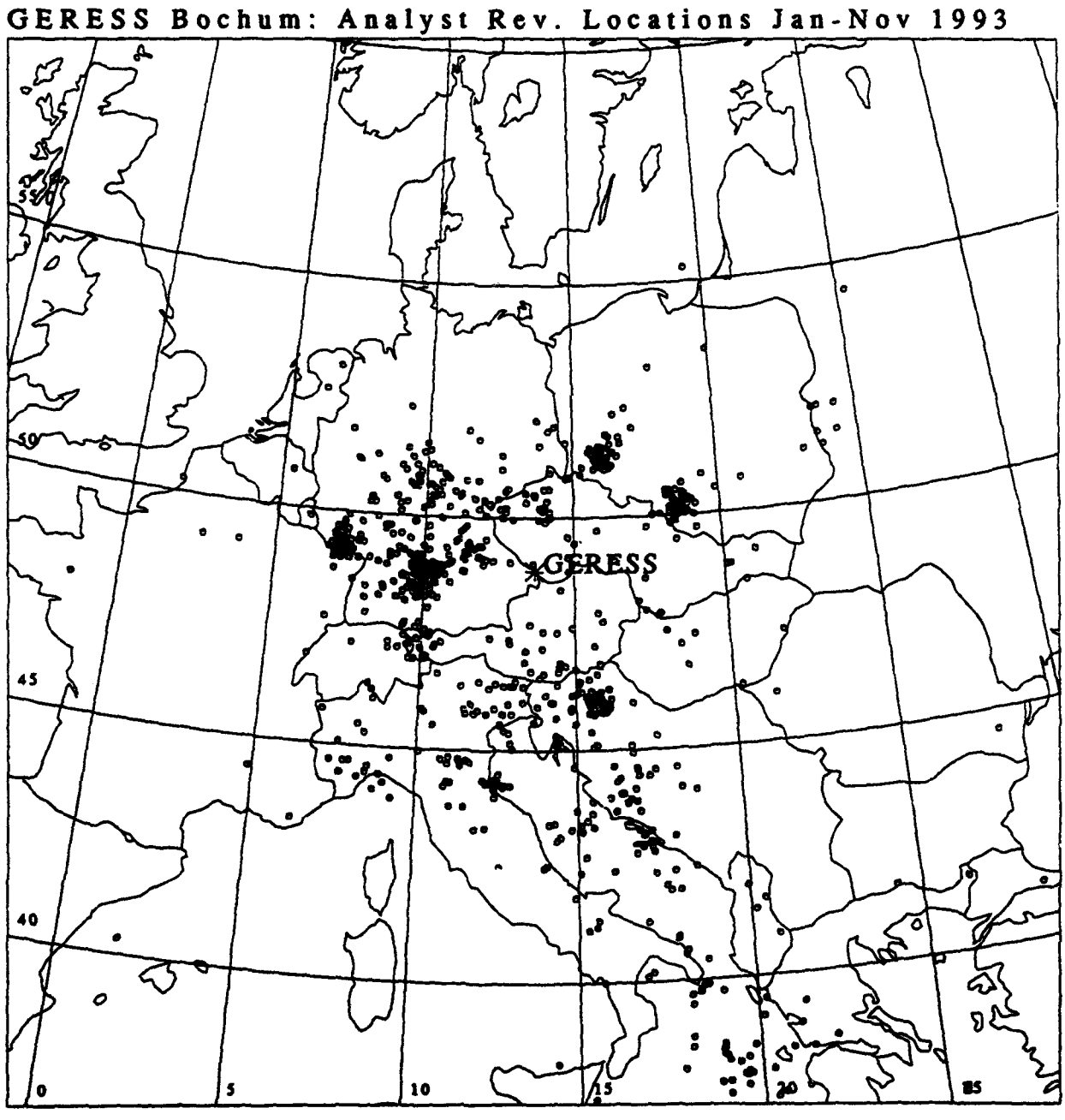
GERESS Bochum: Analyst Rev. Locations Jan-Nov 1993
GERESS
55
50
45
40
0
5
10
15
20
25

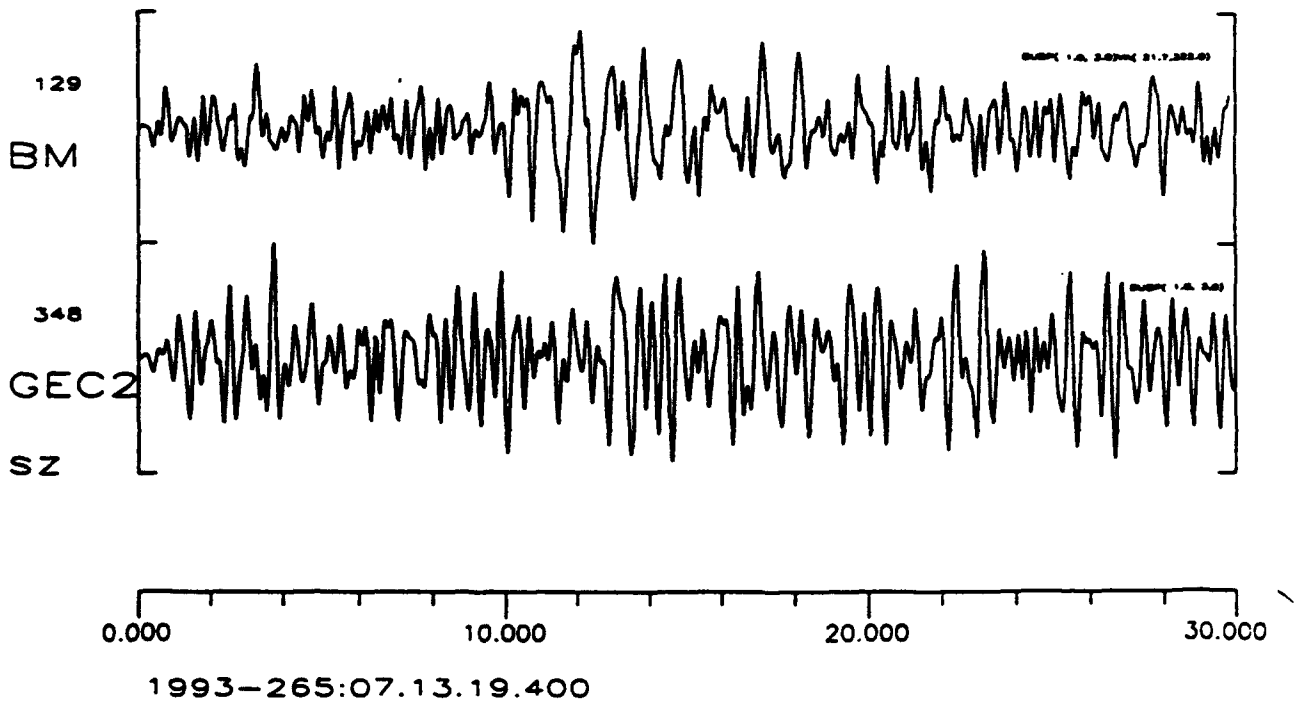

Figure 1-3: GERESS record of the non-proliferation test (NPT) on Sep. 22, 1993, 07:01:080 at NTS (37.202 N and 116.210 W, h= 390 m, elev=1852.5 m). The 1.0 kT yield generated a clear signal at GERESS (Δ = 83.5 deg). At GERESS, a mb = 4.0 was calculated. The figure shows the beam trace (filtered between 1-3 Hz, 5.13 sec/deg, 322 deg) on top and the key station C2 on bottom.

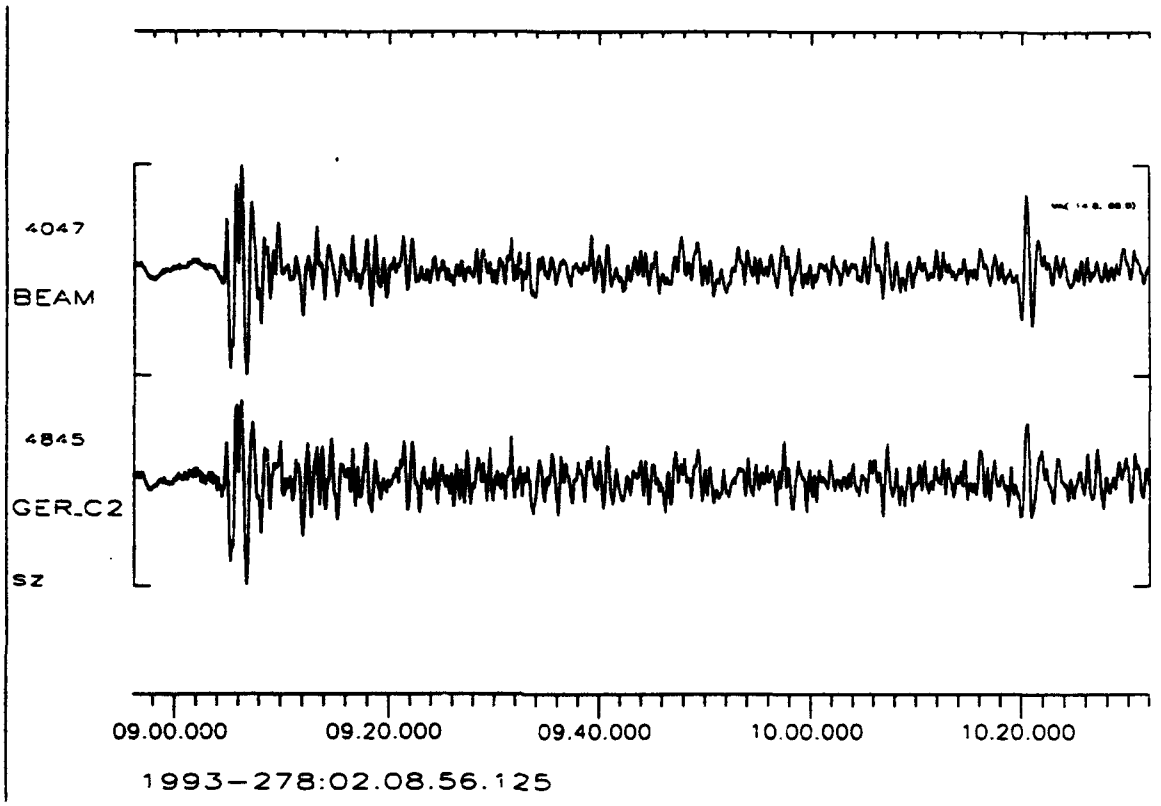

Figure 1-4: GERESS record of the presumed nuclear test at Lop Nor on Oct. 5, 1993, 01:59:56.58, (41.647N 88.681E mb=5.9 PDE weekly). The beam trace (unfiltered, 7.50 sec/deg, 68 deg) is on top and the key station C2 on bottom. Note the PcP onset at 02:10:20.0.

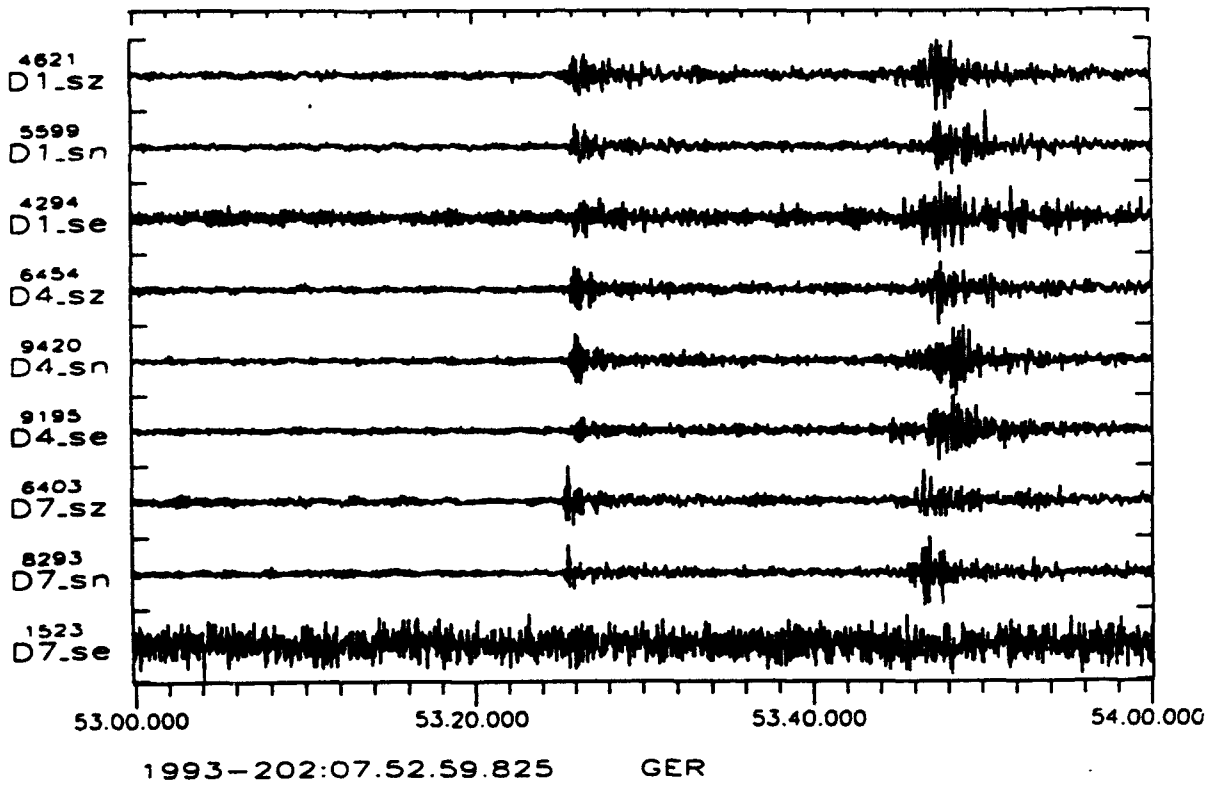

Figure 1-5: GERESS waveform display of D1, D4, and D7 on July 21, 1993 07:52:59. The RDAS-200 occasionally sends electronic noise instead of seismic data after power up or self-reset. This state can be cleared only by manual intervention (reset).

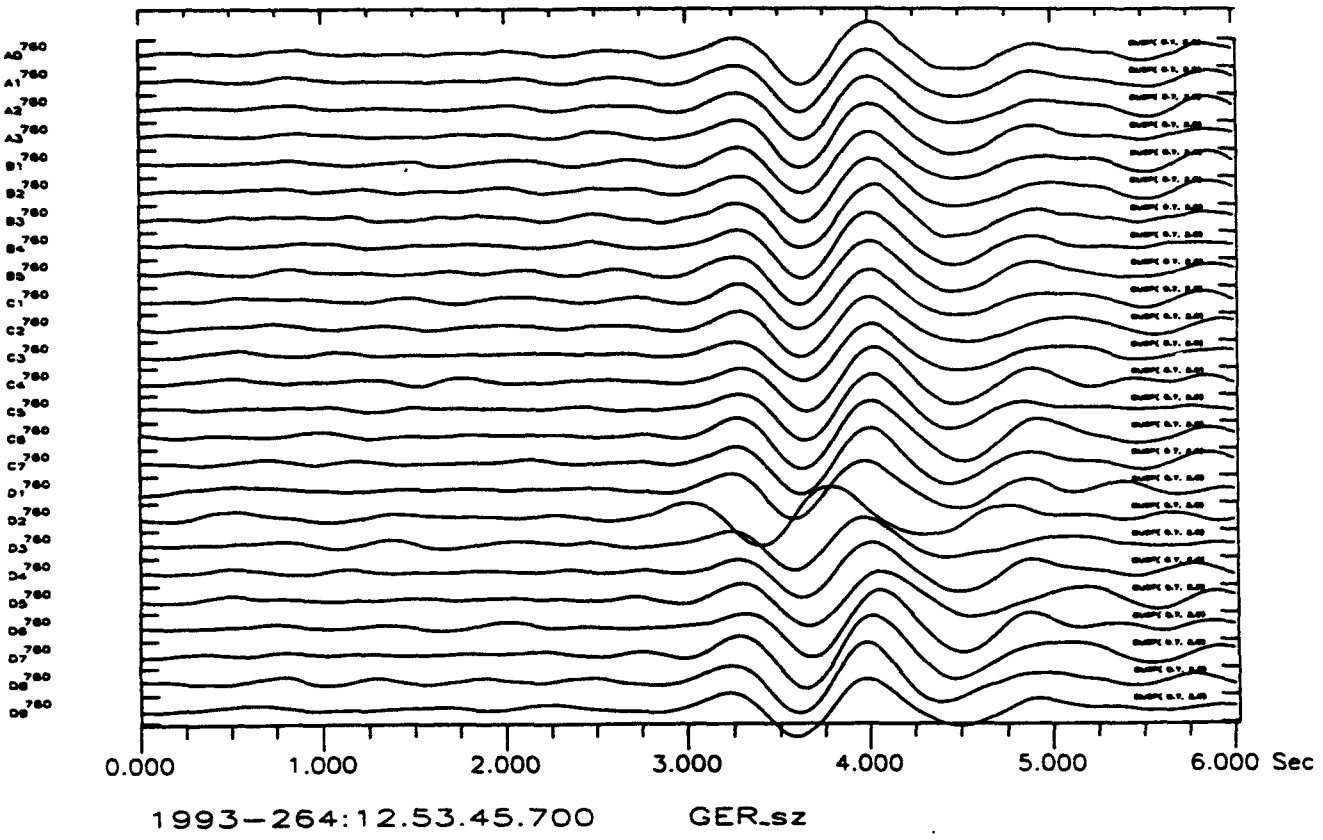

Figure 1-6: GERESS waveform display of all vertical channels on Sep. 21, 1993 12:53:46. The desynchronization of D2 by about 0.2 sec is due to a defective clock module of the RDAS-200. Only an array of RDAS-200s can detect such a timing error. Due to missing spare parts, D2 had been shut down from Sep. 23 - Nov. 19.

2. BLOCKAGE OF REGIONAL SEISMIC WAVES BY THE TEISSEYRE - TORNQUIST ZONE*

Johannes Schweitzer

2.1 Abstract

During the Group of Scientific Experts Technical Test (GSETT, second experiment, 22 April - 2 June 1991) several hundred seismic events were located in Europe. Associating these events to the detecting stations - altogether 28 European stations including 7 arrays participated in the GSETT-2 experiment - clearly shows an influence of the Teisseyre-Tornquist Zone (TTZ) on the propagation of regional seismic phases. Large explosions in the Bay of Gdańsk for example were observed by the well established Scandinavian arrays NORSAR (Δ = 810 km) and ARCESS (Δ = 1670 km) but not by the Polish station KSP (Δ = 470 km) and not at the new high-sensitive GERESS array (Δ = 764 km), both situated south-west of the TTZ. Contrarily, for events in Central Europe with comparable magnitudes we observe a similar decrease of the detection threshold at stations which are located north-east of the TTZ in Scandinavia. To explain these observations, the wave propagation of Pn and Pg crossing perpendicular to the TTZ was modelled with Gaussian beam seismograms. Published crustal models for Poland were used as a starting model for the theoretical seismogram calculations. The observations cannot be explained by a graben-like crustal structure with a jump in Moho depth from 30 km to 50 km. To defocus or damp the seismic energy, the TTZ as a structural anomaly between Eastern and Western Europe must reach down into the upper mantle to a depth of at least about 200 km. The proposed model in this paper is such a deep reaching low velocity body under the TTZ.

2.2 Introduction

The ancient border line between the Precambrian East European Platform with its Palaeozoic cover and the Phanerozoic Central and Western Europe is known as the Teisseyre-Tornquist tectonic zone (Teisseyre, 1893; Tornquist 1908, 1911). The Teisseyre-Tornquist zone (TTZ) is the longest tectonic lineament in Europe. It can be mapped from Southern Scandinavia through Poland to the Black Sea and is one of the most important crustal features in Europe (Mueller and Ansorge, 1989). From several investigations, mostly undertaken in Poland and Southern Scandinavia, it is known that the TTZ is a highly heterogeneous crustal

---

* to be submitted to Geophysical Journal International

structure 20 km to 50 km wide formed during the complex tectonic history of the Caledonian and Variscian orogeneses (e.g. Pożaryski, 1991; Berthelsen, 1992 a, 1992 b; Franke, 1992). The north-west continuation of the TTZ, the Sorgenfrei-Tornquist Zone, was investigated in detail during the European Geotraverse Project (EUGENO-S Working Group, 1988; BABEL Working Group, 1991, 1993).

The structure of the crust on both sides of the TTZ in Poland was investigated with seismic measurements mostly perpendicular to the TTZ (e.g. Guterch et al. 1986; Guterch et al. , 1991). One result of this research during the last 20 years was a detailed picture of the Moho depth in Poland (Fig. 2-1). They proposed a graben like structure of the Moho at the TTZ with a general increase of the crustal thickness from west to east by about 15 km - 20 km. If the results of the reflection and refraction experiments are correct, the Moho has - with more than 50 km in the central part of the TTZ - its greatest depth for whole Europe (Meissner et al. , 1987). The increase of the lithospherical thickness from the Phanerozoic part of Europe to the Precambrian Platform is confirmed by surface wave inversion studies (Snieder, 1988; Zielhuis, 1992) and S-wave travel times tomography (Zielhuis, 1992). Additionally, these authors proposed deeper reaching structural differences between the western and the eastern part of Europe. They found evidence for a boundary along the TTZ with respect to standard Earth models in the uppermost 200 km of the upper mantle. In the following study, the blockage of regional seismic waves due to the TTZ will be shown and discussed.

2.3 The observations

In 1991 (22. April - 2. June) the international data exchange experiment GSETT-2 of the Geneva Group of Scientific Experts (GSE) took place. One goal of the GSETT-2 experiment was to detect and locate the global seismicity expeditiously 57 seismic stations participated in the experiment with a concentration in Europe, where 27 stations or arrays sent full wave form data and / or parameter readings of all detected onsets to the Experimental International Data Centers. The results of GSETT-2 were compiled in daily Final Event Bulletins (FEB's) which were produced with only one week delay. Locations of several hundreds of seismic sources - natural or artificial - in Europe can be found in the FEB's. Because the FEB's were produced under strong time pressure, several mislocations and misassociations can be found in these bulletins. In this study, all events in and around Europe were checked carefully and the FEB's were cleaned from obviously erroneous associated onsets and events. Fig. 2-2 shows the TTZ and all stations in Europe which participated in GSETT-2.

Due to the concentration of highly sensitive seismic stations in Central and Northern Europe, the large number of events from mining activities and / or quarry blasting dominates the seismicity map of this region. So, the GSETT-2 experiment clearly showed the advantage of high sensitive stations and regional arrays for monitoring a test ban treaty for nuclear tests. This was especially true for the new small aperture array in Germany, the GERman Experimental Seismic System

(GERESS) (Harjes, 1990), which has become the most sensitive seismic station in Central Europe (Schweitzer et al. , 1992). But surprisingly, this array has not detected any of the events north-east of the TTZ. Consequently, a systematic investigation of the station detectability was untertaken (Gestermann et al. 1991; Schweitzer et al. , 1992).

In Fig. 2-3-a all reviewed events (maximum likelihood FEB-magnitude of $\geq$ 3.0, epicentral distance $\Delta \leq 15°$ from the station) are shown which have been detected by stations south-west of the TTZ, and Fig. 2-3-b shows all events which have been detected by stations north-east of the TTZ. Obviously, the TTZ influences the detectibility of seismic events. The events of four source regions, namely I quarries in Estonia and Russia, II events in the Bay of Gdańsk, III Polish copper mine area, and IV Polish coal mine area, play a major rôle in the following discussion.

The detection capabilities of the four small aperture seismic arrays in Europe (ARCESS, FINESA, GERESS, and NORESS are indicated with their reference stations respectively) and the Polish station KSP will be compared with the theoretically observable events at these stations. Fig. 2-4 shows the influence of the TTZ on the detection capability of the GERESS array. The theoretically observable events are plotted (Fig. 2-4-a) against the theoretical backazimuth (BAZ) at GERESS and the epicentral distance from GERESS. Additionally, the position of the TTZ is shown in this projection. For better orientation, the Roman numerals show the four source regions of Fig. 2-3. In Fig 4-b, all events are plotted for which GERESS detected at least one onset. Clearly seen is the shadow of the TTZ, the source regions I and II were not observed with GERESS although most of the events in the same distance range in other directions (BAZ between about 100° and 315°) could be detected. To prove this result, original data of the GERESS array have been retrieved and no associatable phase could be found even for the strongest events in source regions I and II.

The opposite situation can be observed at the Scandinavian arrays: Fig. 2-5 shows the detection capability of the NORESS array in southern Norway. Now the source regions III and IV in the Silesian mining areas and the large quarry activity in the Czech Republic and in Germany are not observed, contrary to the quarry activities in Finland and northern Sweden, which occurred at similar distance ranges. As in the case of NORESS, the detectibility of FINESA (Fig. 2-6) is also influenced by the TTZ.

The situation for the ARCESS array (Fig. 2-7) is more complicated because the distance between ARCESS and the TTZ is much larger (i.e. twice the distance between NORESS and the TTZ). Because there is no other such highly sensitive station in this distance range from the TTZ, the effect of amplitude decay of seismic energy due to geometrical spreading and attenuation cannot be separated from the assumed blockage effect due to the TTZ. Additionally, rays for P-phases from source regions III and IV are diving deeply into the upper mantle and are probably not influenced by the TTZ. However, the detection of events in source region II in the Bay of Gdańsk by the ARCESS array at a distance of about 1700 km is remarkable because these events were not detected by GERESS at a distance of about 700 km (s. Fig. 2-4).

Finally, the influence of the TTZ on the detection capability of the three-component station KSP in Poland is shown in Fig. 2-8. Although this single station

generally has a lower sensitivity than the arrays, it is surprising that the events of source region II in an epicentral distance of about 500 km are not detected (contrary to ARCESS in 1700 km, FINESSA in 850 km, and NORESS in 800 km).

All these observations can only be explained with a blockage of seismic phase propagation due to the TTZ.

2.4 The model

The two seismic stations GERESS and KSP and the two source regions in the border region between Estonia and Russia (I) and in the Bay of Gdańsk (II) are approximately located on a great circle path perpendicular to the TTZ. Fig. 2-9 shows the stations, the source regions, and the profile. In the following, a velocity model for this profile will be deduced which is based on results of the deep seismic sounding International Profile VII (Guterch et al., 1975, 1986) which was shot parallel to the discussed profile. Calculating theoretical seismograms for TTZ-structures aimed at decreasing the amplitudes of seismic phases in such a way that seismic energy from source regions I and II would not be detectable at the stations GERESS and KSP. The modelling of the TTZ was limited to P-velocity structure assuming that a shadow of Pn-phases and Pg-phases also explains the shadow of Sn-phases and Sg-phases. The blockage of Lg-phases by the TTZ does not need to be modelled, because it is known that a laterally heterogeneous crust with additionally changes in the crustal thickness very effectively suppress Lg-wave propagation (e.g. Kennett, 1986; Kennett, 1989; Cao and Muirhead, 1993). All theoretical seismograms for modelling the TTZ were calculated with a Gaussian beam program packet (Weber, 1988) and including the Earth flattening approximation after Müller (1977).

At first, the wave propagation of Pg and Pn was studied for a laterally homogeneous model (Fig. 2-10), which is based on the slightly smoothed P-velocity model MUMEP of the East European Platform (Grad, 1987). The S-velocities were calculated from the P-velocities with the standard Poisson-ratio of 0.25, Q-structure and densities were adopted from PREM (Dziewonski and Anderson, 1981). Fig. 2-11 shows all ray paths through this model which have been used for calculating the theoretical seismograms. An explosion point source was assumed at source region I (1667 km) at the north-east end of the profile. The positions of the seismic station KSP (402 km) and the GERESS array (212 km) are marked. Beside the standard phases Pn and Pg, several reverberations of these phases in the crust, reflections at the Earth's surface, and some P-SV conversions have been added to calculate the theoretical seismograms. A comparison with theoretical seismograms calculated with the reflectivity method for the same 1D model showed that thi- combination of phases is a good approximation of the full wavefield of the P-wave group. In Fig. 2-12, the theoretical seismograms calculated with the Gaussian beam method for a model of the East European Platform are shown. The used program packet to calculate Gaussian beam seismograms give no information about

absolute amplitudes, but relative amplitudes in one seismogram section are correct and can be used for comparison. In Fig. 2-12, all seismograms have been normalised relative to the maximum amplitude of the seismogram in 700 km; the positions of KSP and GERESS are marked again. The seismogram section reflects the good conditions for P-wave propagation in the Precambrian East European Platform and partly explains the high detection capability of the Scandinavian arrays for events in Eurasia.

In the next step, the TTZ with its crustal structure and Moho depth as deduced by Guterch et al. (1975, 1986) for International Profile VII was included in the central part of the model. In the north-eastern part of the profile, the model of the East European Platform remained unchanged, but in the south-western part an IASP91-like crust and upper mantle was modelled (Kennett and Engdahl, 1991). This model accounts for the increase in crustal thickness from Western to Eastern Europe as indicated by several studies. For the seismological evidence see e.g. Snieder (1988) or Zielhuis (1992), heat flow data can be found e.g. in Čermák et al. (1989) or in Plewa (1991), and magnetic and gravity data are presented e.g. in Grobawska et al. (1991). The S-velocities have been changed, respectively, densities and Q-structure were not changed. The P-velocity structure of this model can be seen in Fig. 2-13. The most prominent feature of this first model is the graben like structure of the TTZ with a Moho depth between 50 km and 60 km in the central part of the profile. The ray tracing results for this model are shown in Figs. 14 a+b for the two source regions respectively. Theoretical seismograms calculated with the Gaussian beam method are shown in Figs. 15 a+b, again for both source regions. The seismograms are normalised as in Figs. 12 to the maximum amplitude of the seismogram in 700 km.

As expected, the crustal structure and the Moho topography effectively obstruct the wave propagation in the crust. Shortly beyond the TTZ, only phases with low amplitudes which propagate as multiple phases through the crust can be observed. This crustal model with an assumed change in crustal thickness between the East European Platform and Western Europe can explain the observed shadow for events from source region II in the Bay of Gdańsk at stations south-west of the TTZ. But the picture for Pn-waves - i.e. energy travelling through the uppermost part of the mantle - looks different. Although the graben like structure of the Moho below the TTZ produces some shadow effect, Pn and its multiples are still observable at the station KSP and the GERESS array for events occurring at source region I (Fig. 2-15a). This is a clear evidence that the shadow effect of the TTZ is not only a result of the crustal structure of this ancient border line through Europe, but also an effect of the structure in the uppermost mantle, and that the border between the two parts of Europe reaches deeper than the Moho discontinuity. This leads to a further modification of the P-velocity model for the TTZ.

Starting from the model in Fig 13, a second model was derived with a trial and error search which can fit the observed shadow produced by the root of the TTZ. The P-velocity structure of this model is shown in Fig. 2-16. The crustal structure of this model is the same as in Fig. 2-13, but the velocities in the uppermost mantle below the TTZ had to be changed to explain the observed shadow. The major change is the low velocity under the Moho graben of the TTZ. These velocities are lower than in the model of the East European Platform (s. Fig. 2-10)

and also lower than the standard velocity model like IASP91 (s. the left part of Fig. 2-13). Our final velocity model leads to a defocusing of the P-waves in the uppermost mantle and to the desirable shadow zone (Figs. 17 a+b). Figs. 18 a+b show the theoretical seismograms calculated for this model which confirm the ray tracing results: neither KSP nor GERESS observe a P-wave.

2.5 Discussion

Our final model of the P-velocity structure for of the TTZ including a low velocity zone down to about 200 km can explain the observed shadow effect of the TTZ. On the other hand, our model also produce some focusing effects at larger distances from the TTZ as indicated by the ray pictures (Figs. 17 a+b). It is an open question at the moment, whether this energy can be observed with high sensitive stations positioned on the profile elongated to the south-west in the Alps. The proposed model of the TTZ is not symmetric and theoretical seismogram calculations for a reversed geometry (source south-west and stations north-east of the TTZ) - not presented in this paper - show that the shadow of the TTZ in north-east direction is not as pronounced as in south-west direction. This explains without further modelling the fact that the Scandinavian arrays north-east of the TTZ are not totally blind for events beyond the TTZ in Central Europe (s. Figs. 5 - 7).

The proposed low velocity zone can effectively defocuses the seismic energy, but this is not the only model to explain the blockage of seismic energy propagation due to the TTZ. Another possibility would be e.g. changes of the seismic impedance along first order discontinuities where P-waves would be reflected somewhere in the mantle. Alternatively, seismic energy could be damped by a low Q-structure below the TTZ, but only very low effective Q-values were able to model the observed shadow. Such extremely low Q-models are rather unlikely. Whatever the structure of the deeper TTZ might be, the result of modelling the amplitudes of regional seismic waves clearly shows that the TTZ effects seismic waves down to at least 200 km depth.

Literature

BABEL Working Group, 1991. Deep seismic survey images crustal structure of Tornquist Zone beneath southern Baltic Sea, *Geophys. Res. Lett.* **18**, 1091 - 1094.

BABEL Working Group, 1993. Deep seismic reflection / refraction interpretation of crustal structure along the BABEL profiles A and B in the southern Baltic Sea, *Geophys. J. Int.* **112**, 325 - 343.

Berthelsen, A., 1992a. Mobile Europe, in: *A continent revealed - The European Geotraverse*, pp. 17 - 32, ed. Blundell, D., Freeman, R. & Mueller St., Cambridge University Press, Cambridge.

Berthelsen, A. 1992b. From Precambrian to Variscian Europe, in: *A continent revealed - The European Geotraverse*, pp. 153 - 164, ed. Blundell, D., Freeman, R. & Mueller St., Cambridge University Press, Cambridge.

Cao, S. & Muirhead, K. J., 1993. Finite difference modelling of Lg blockage, *Geophys. J. Int.* **115**, 85-96.

Čermák, V., Šafanda J. & Guterch, A. 1989. Deep temperature distribution along three profiles crossing the Teisseyre-Tornquist tectonic zone in Poland, *Tectonophysics* **164**, 151 - 163.

Dziewonski, A. M. & Anderson, D. L., 1981. Preliminary reference Earth model. *Phys. Earth Planet. Inter.* **25**, 297-356.

EUGENO-S Working Group, 1988. Crustal structure and tectonic evolution of the transition between Baltic Shield and the North German Caledonides (the EUGENO-S Project), *Tectonophysics* **150**, 253 - 348.

Franke, W. 1992. Phanerozoic structures and events in Central Europe, in: *A continent revealed - The European Geotraverse*, pp. 164 - 180, ed. Blundell, D., Freeman, R. & Mueller St., Cambridge University Press, Cambridge.

Gestermann, N., Jost, M. L., & Schweitzer J. 1991. Performance of the new German Experimental Regional Seismic System (GERESS) during GSETT-2, *EOS, Trans. Amer. Geoph. Union* **72**, 345 (abstract).

Grad, M. 1987. Seismic model of the Earth's crust and upper mantle of the East European Platform, *Acta Geophysica Polonica* **35**, 121 - 155.

Grobawska, T., Koblański, A., & Dolnicki, J., 1991. Deep structure of the Earth's crust in the Teisseyre-Tornquist Zone (TTZ) in Poland, based on magnetic and gravity studies, *Publs. Inst. Geophys. Pol. Acad. Sc.* **A-20 (255)**, 81 - 89.

Guterch, A., Materzok, R., Pajchel, J. & Perchuć, E., 1975. Crustal structure from deep seismic sounding along International Profile VII on the territory of Poland, in *Proceedings 14. General Assembly ESC Trieste*, pp. 281 - 293, ed. Stiller, H., Berlin.

Guterch, A., Grad, M., Materzok, R., Pajchel, J., Perchuć, E. & Toporkiewicz, St., 1984. Deep structure of the Earth's crust in the contact zone of the Paleozoic and Precambrian Platforms and the Carpathian Mts. in Poland, *Acta Geophysica Polonica* **32**, 25 - 41.

Guterch, A., Grad, M., Materzok, R. & Perchuć, E., 1986. Deep structure of the Earth's crust in the contact zone of the Palaeozoic and Precambrian Platforms in Poland (Tornquist - Teisseyre Zone), *Tectonophysics* **128**, 251 - 279.

Guterch, A., Grad, M., Materzok, R., Perchuć, E., Janik, T., Gaczyński, E., Doan, T., Bialek, T., Gadomski, D., Młynarski, St. & Toporkiewicz, St., 1991. Structure of the lower crust of the Paleozoic Platform in Poland from seismic wide-angle and near-vertical reflection surveys, *Publs. Inst. Geophys. Pol. Acad. Sc.* **A-19 (236)**, 41 - 62.

Harjes, H.-P., 1990. Design and siting of a new regional seismic array in Central Europe, *Bull. Seism. Soc. Am.* **80**, 1801 - 1817.

Kennett, B. L. N., 1986. Lg-waves and structural boundaries, *Bull. Seism. Soc. Am.* **76**, 113- 1141.

Kennett, B. L. N., 1989. Lg-wave propagation in heterogeneous media, *Bull. Seism. Soc. Am.* **79**, 860 - 872.

Kennett, B. L. N. & Engdahl, E. R., 1991. Travel times for global earthquake location and phase identification, *Geophys. Journ. Int.* **105**, 429 - 466.

Meissner, R., Wever, Th. & Flüh, E. R., 1987. The Moho in Europe - Implications for crustal development, *Annales Geophysicae* **5B**, 357 - 364.

Müller, G., 1977. Earth flattening approximation for body waves derived from geometric ray theory - improvements, corrections and range of applicability, *Journ. Geophys.* **42**, 429-436.

Mueller, St. & Ansorge J., 1989. The crustal structure of Western Europe, *Ann. Rev. Earth Planet. Sci.* **17**, 335 - 360.

Plewa, M., 1991. The heat flow on the Polish territory, *Scientific Bulletins of the Stanislaw Staszic Academy of Mining and Metallurgy* **1373**, Applied geophysics **8**, 141 - 151.

Pożaryski, W., 1991. The strike-slip terrane model for the North German-Polish Caledonides, *Publs. Inst. Geophys. Pol. Acad. Sc.* **A-19 (236)**, 3 - 12.

Schweitzer, J., Jost, M. L. & Gestermann N., 1992. GERESS - A new array for on-line monitoring the regional seismicity in Central Europe, *Cahiers du Centre Européen de Géodynamique et de Séismologie* **5**, 1 - 10.

Snieder, R., 1988. Large scale waveform inversions of surface waves for lateral heterogeneity. 2. Application to surface waves in Europe and the Mediterranean, *Journ. Geophys. Res.* **93**, 12067 - 12080.

Teisseyre, W., 1893. Calokstalt plyty paleozoicznej Podola galicyjskiego. Rzecz o przyszlych wierceniach glebokich na Podolu opolskim, *Kosmos* **18**, 319 - 336 (in polish).

Tornquist, A., 1908. Die Feststellung des Südwestrandes des baltisch-russischen Schildes und die geotektonische Zugehörigkeit der ostpreußischen Scholle, *Schriften der Physikalisch-ökonomischen Gesellschaft* **49**, Heft 1, 12 pp.

Tornquist, A., 1911. Die Tektonik des tieferen Untergrundes Norddeutschlands, *Sitzungsberichte der Königlich Preußischen Akademie der Wissenschaften* **38**, 822 - 836.

Weber, M., 1988. Computation of body-wave seismograms in absorbing 2-D media using the Gaussian beam method: comparison with exact methods, *Geophys. Journ. Int.* **92**, 9-24.

Zielhius, A., 1992. S-wave velocity below Europe from delay-time and waveform inversions, PhD thesis, Rijksuniversiteit Utrecht, Geologica Ultraiectina **88**, 148 pp, Utrecht.

ACKNOWLEDGEMENTS

I thank H.-P. Harjes for his continuing encouragement during this work and a careful review of the manuscript. Constructive discussions with Nicolai Gestermann and Michael L. Jost are acknowledged. Fig. 2-3 was compiled by M. L. Jost, for Fig. 2-4 - Fig. 2-8 I thank N. Gestermann for his help and Vera Schulte-Pelkum for a correction of the manuscript. A critical review of this paper and hints for calculating the Gaussian beams by Michael Weber are acknowledged.

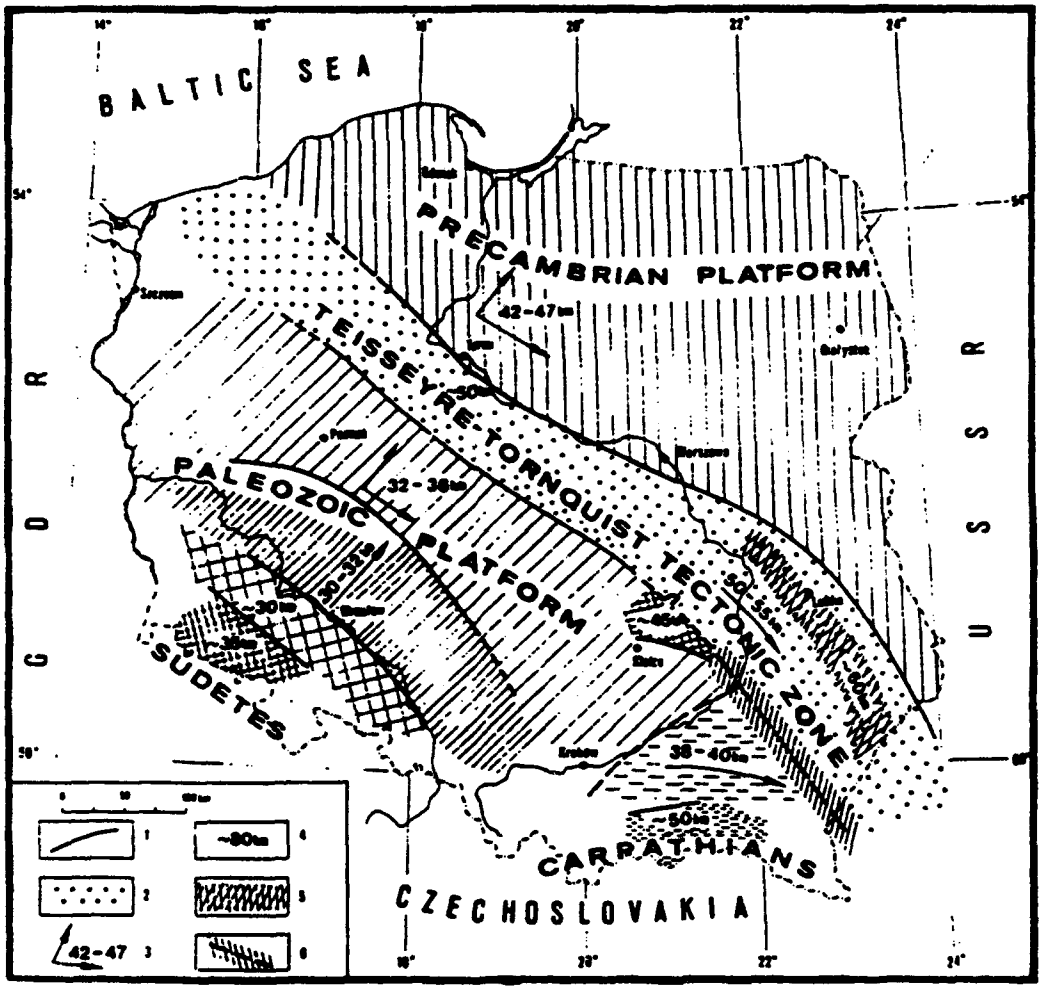

Fig. 2-1: Tectonic map of Poland with the Teisseyre-Tornquist Zone. 1 - boundaries of crustal blocks, 2 - Teisseyre-Tornquist Zone (TTZ), 3 and 4 - depth of the Moho discontinuity and directions of increase of thickness of the Earth's crust in kilometres, 5 - anomalous zone in crustal structure in the TTZ, 6 - boundaries of crustal blocks determined approximately (all from Guterch et al., 1984).

Fig. 2-2: All seismic stations and arrays in Europe which participated in the GSETT-2 experiment in 1991, additionally mapped is the TTZ.

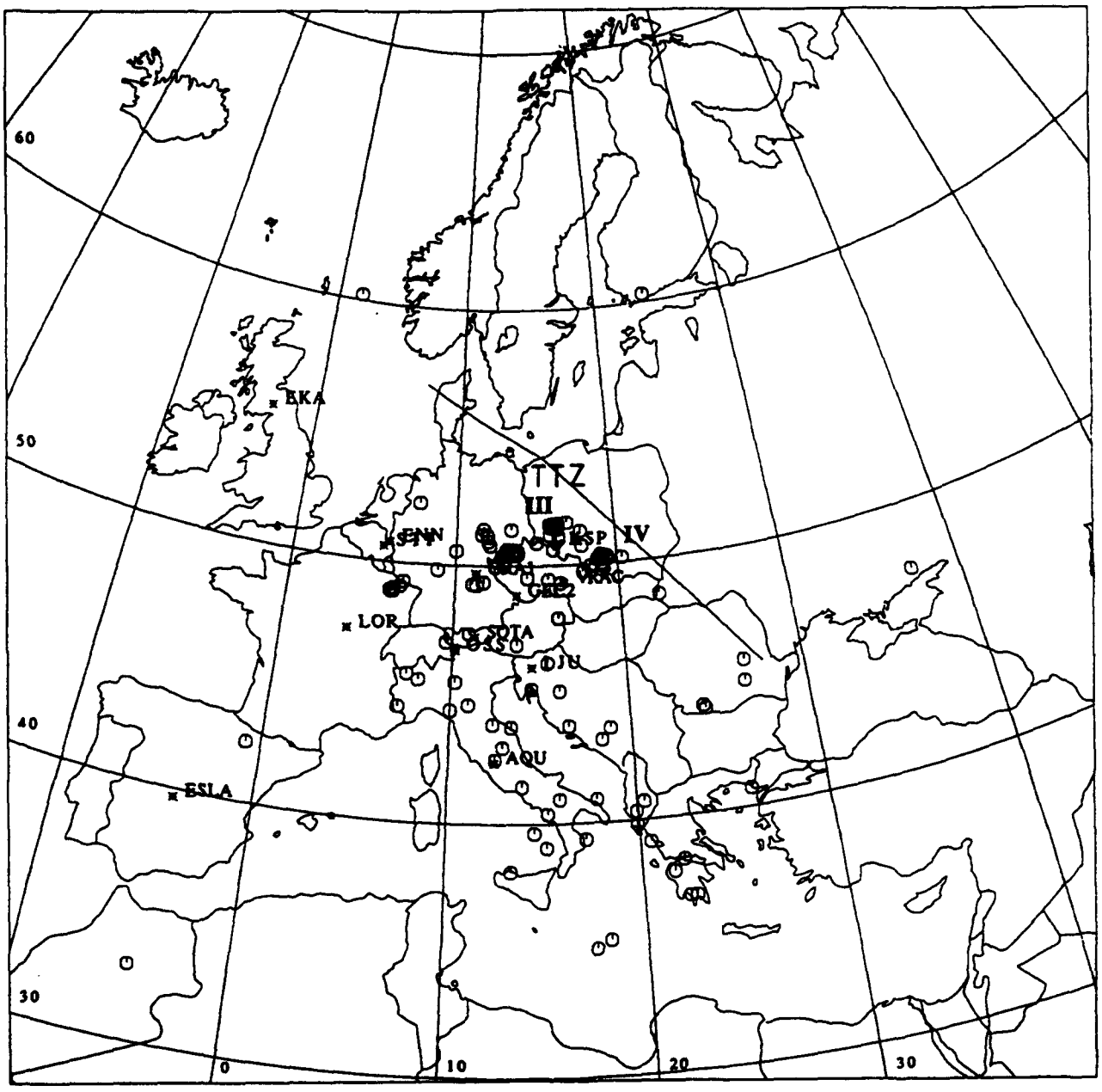

a

Fig. 2-3: a) All FEB-events ($m_b \geq 3.0$) detected by seismic stations or arrays (s. Fig. 2-2) south-west of the TTZ in an epicentral distance $\Delta \leq 15°$ respectively. b) as Fig. 2-3-a, but all FEB-events which had been detected by seismic stations or arrays north-east of the TTZ. The Roman numerals indicate four source regions wich had been investigated in more detail.

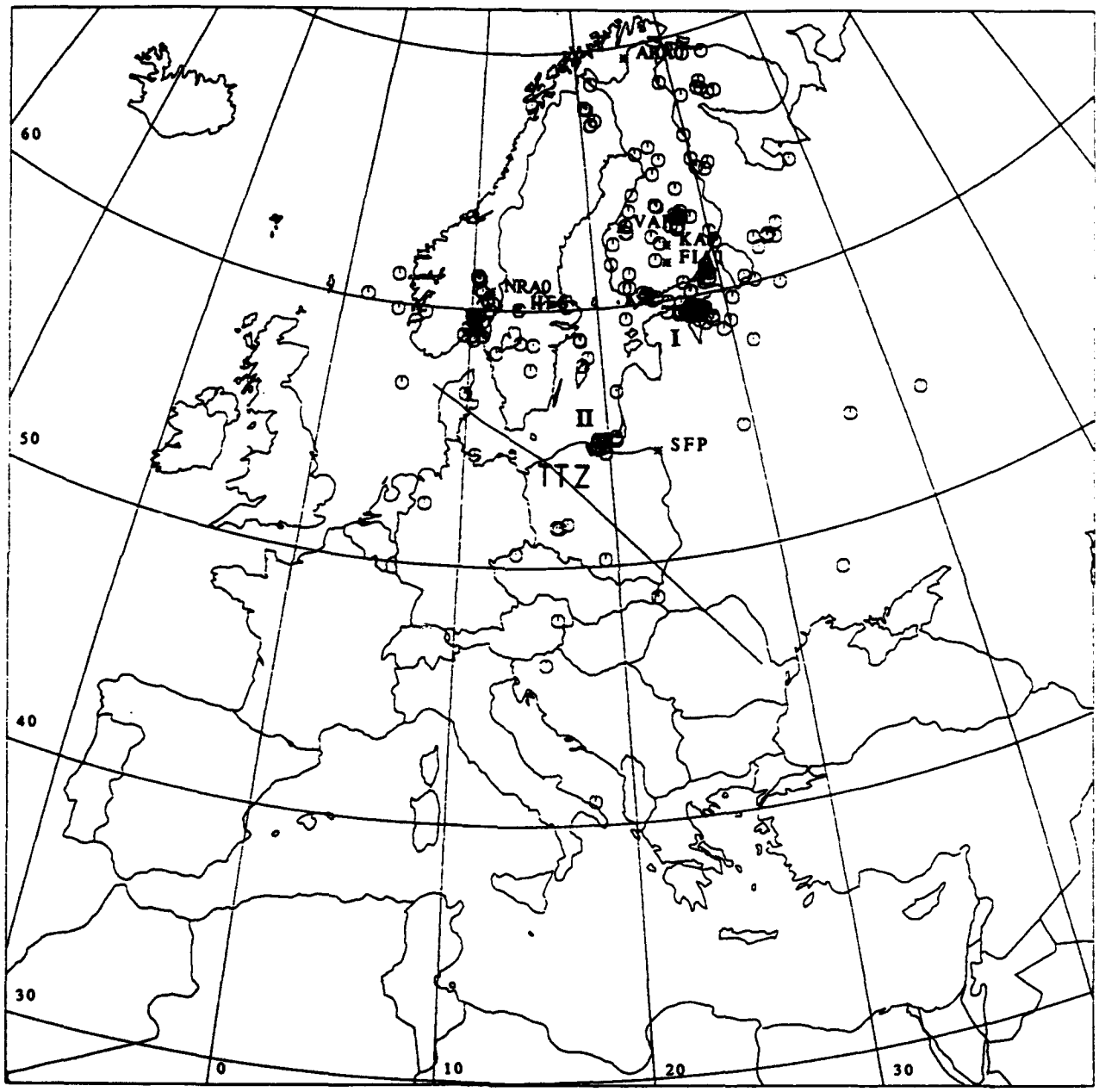

b

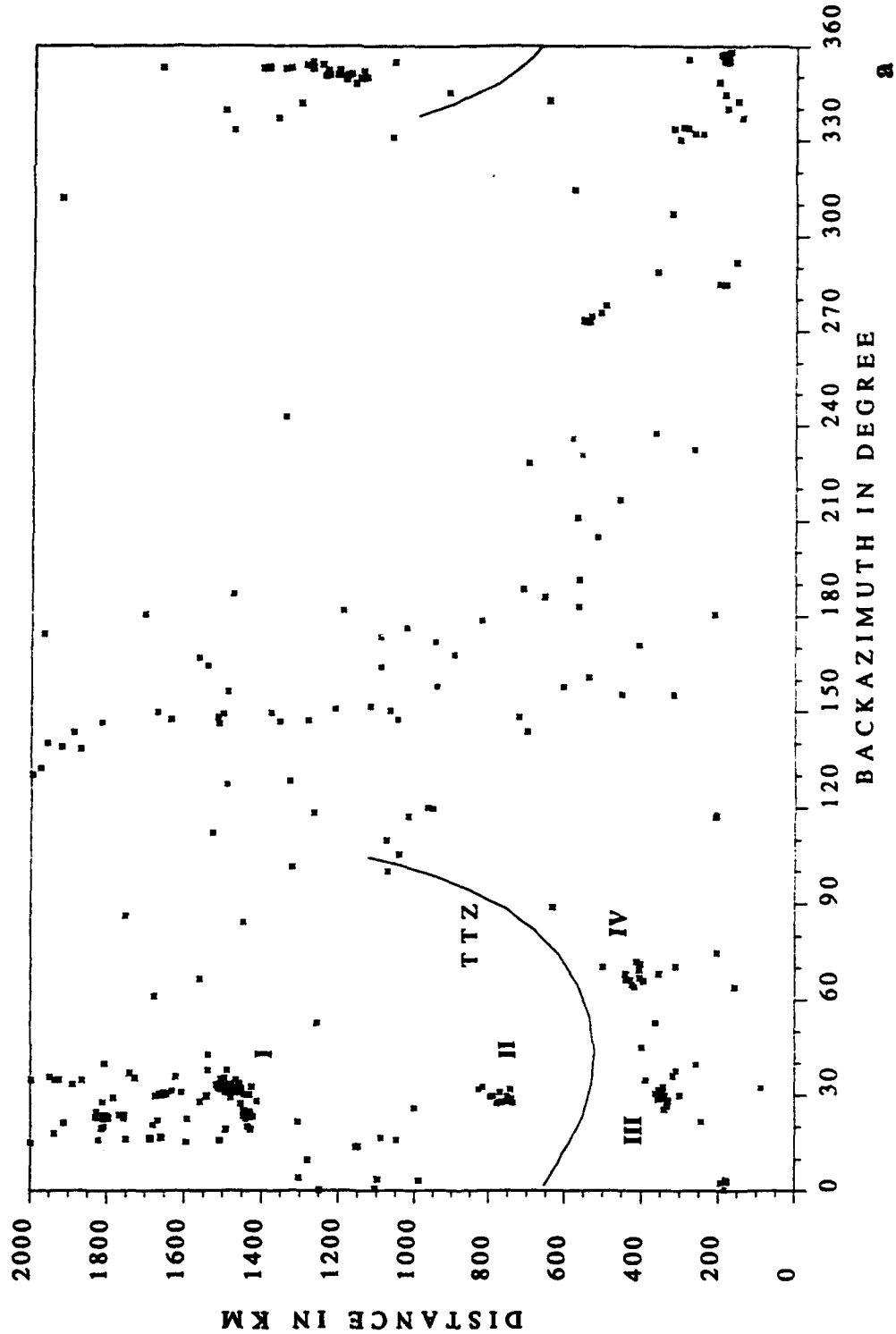

Fig. 2-4: a) All 333 FEB-events with a FEB magnitude ≥ 3.0 which occurred in a distance of 2000 km around the GERESS-array. The events are shown with respect to the backazimuth from GERESS. Additionally shown is the position of the TTZ in this projection. b) As in Fig. 2-4-a, but only the 117 events are plotted, for which the GERESS array had detected at least one seismic phase. The Roman numerals indicate the four source regions (for details see text).

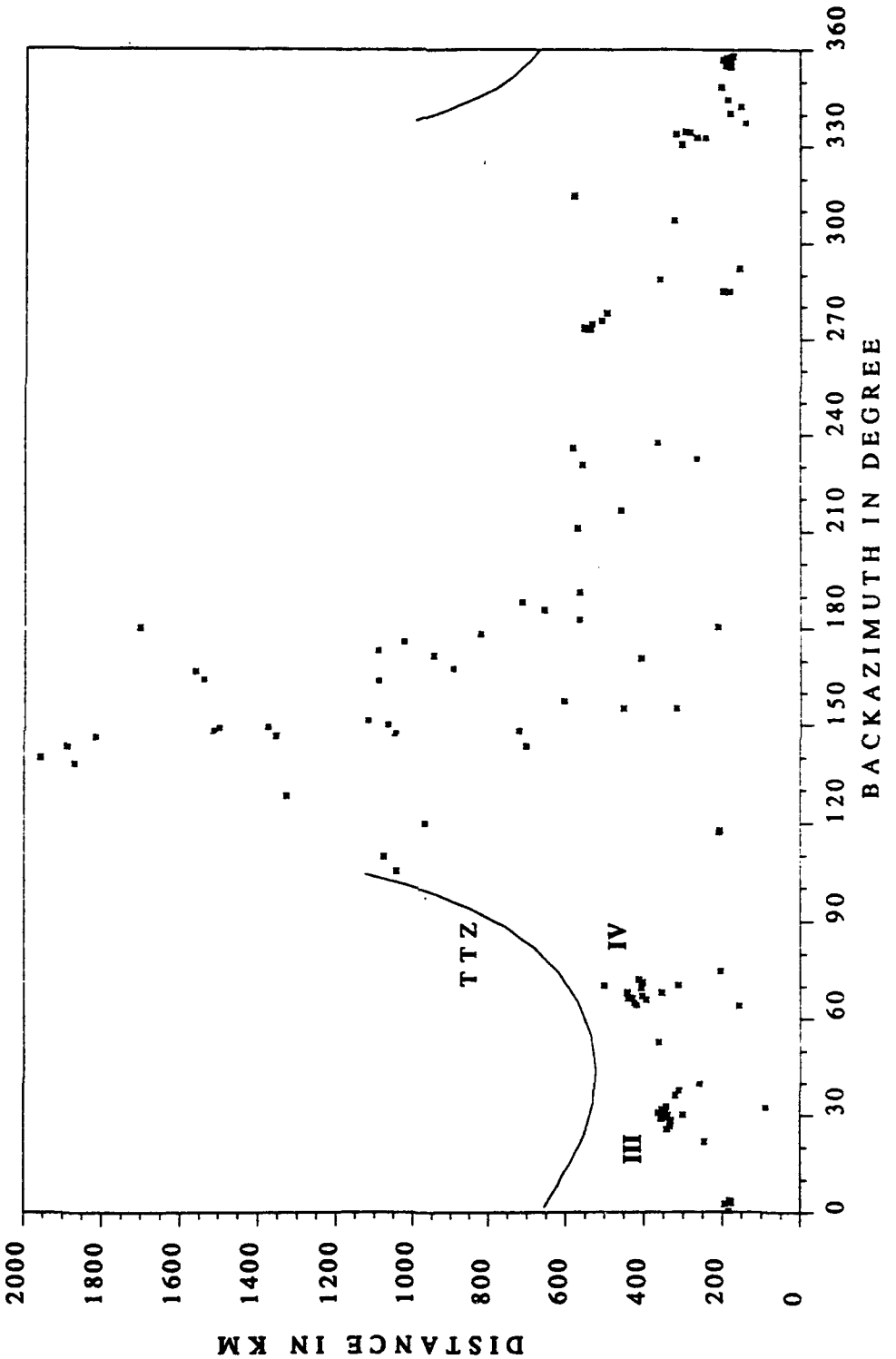
DISTANCE IN KM
2000
1800
1600
1400
1200
1000
800
600
400
200
0
BACKAZIMUTH IN DEGREE
0
30
60
90
120
150
180
210
240
270
300
330
360
TTZ
III
IV

b

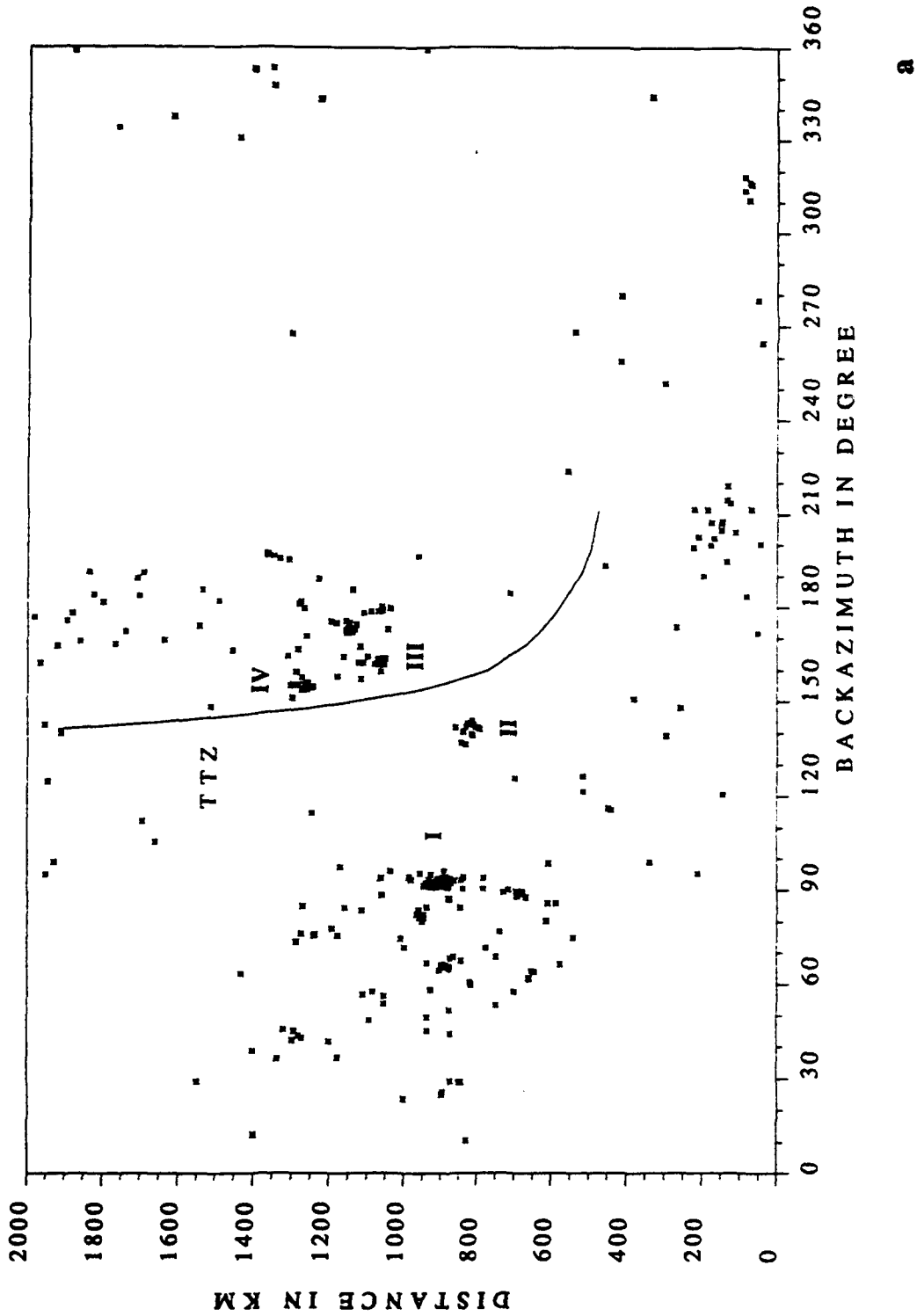

Fig. 2-5: as Fig. 2-4, but for the NORESS array. (151 of 326 events were detected)

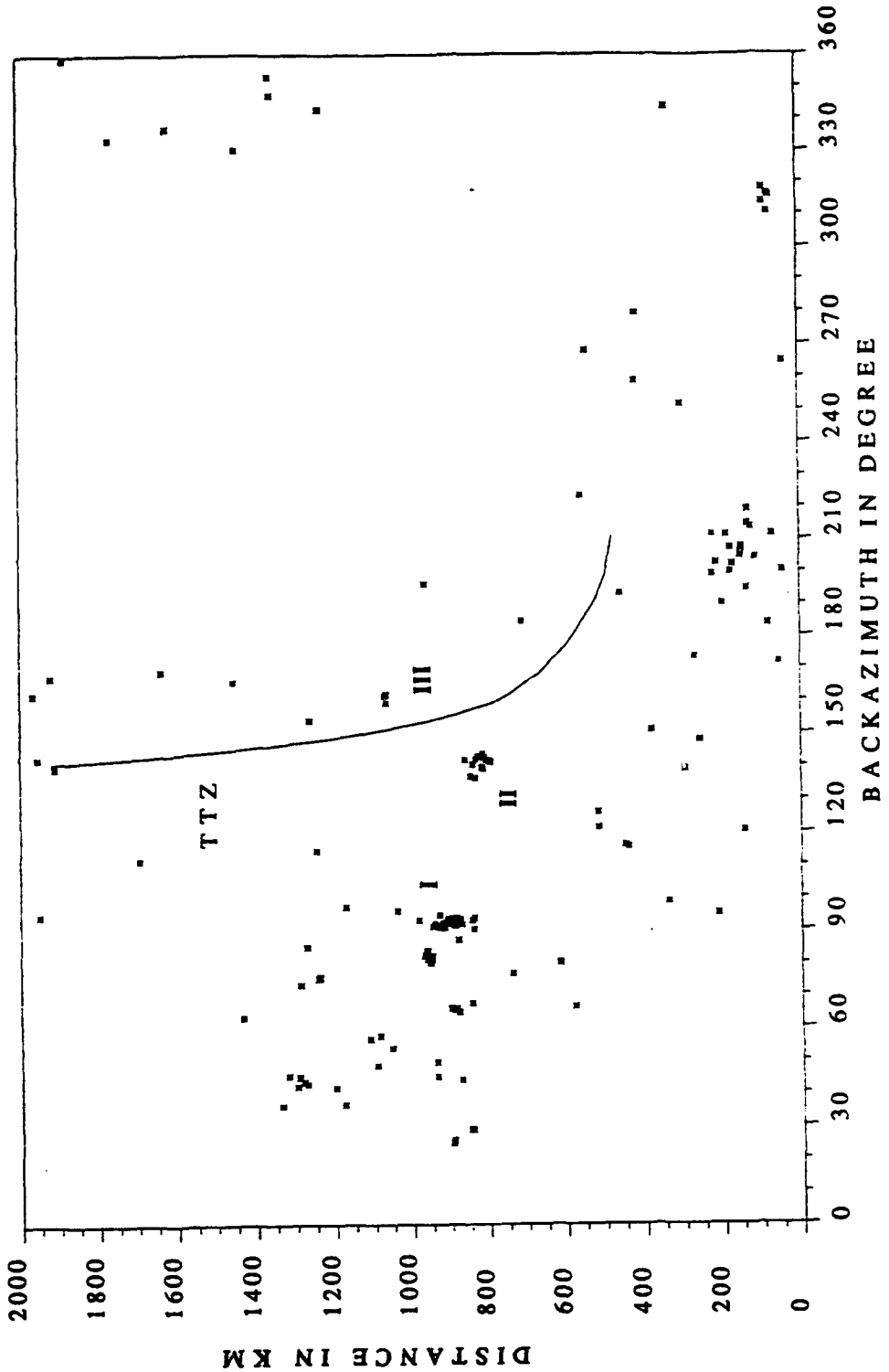
DISTANCE IN KM
2000
1800
1600
1400
1200
1000
800
600
400
200
0
BACKAZIMUTH IN DEGREE
0
30
60
90
120
150
180
210
240
270
300
330
360
TTZ
I
II
III

b

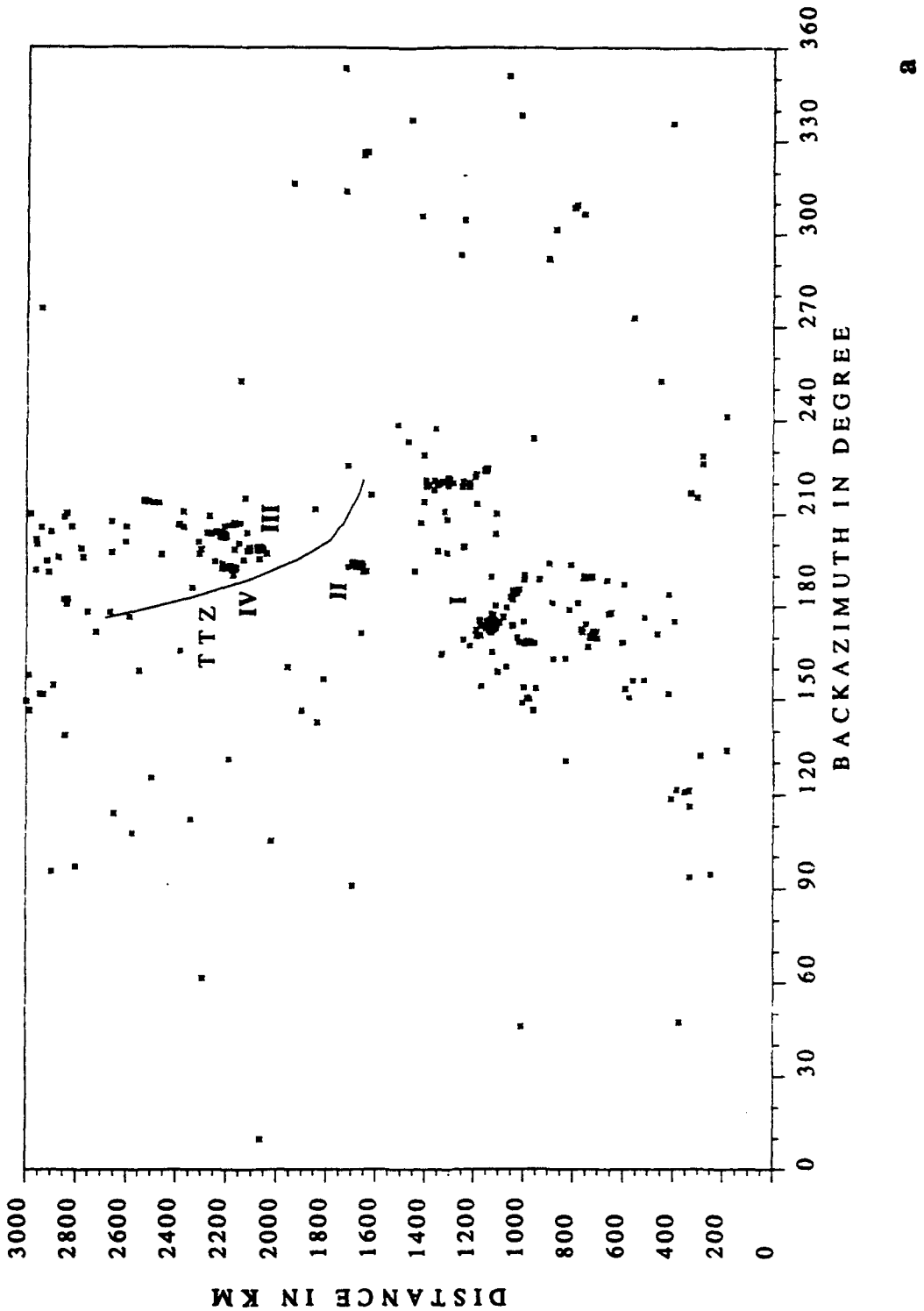

Fig. 2-6: as Fig. 2-4, but for the ARCESS array. Note, that for ARCESS all events up to an epicentral distance of 3000 km are plotted. (155 of 360 events were detected)

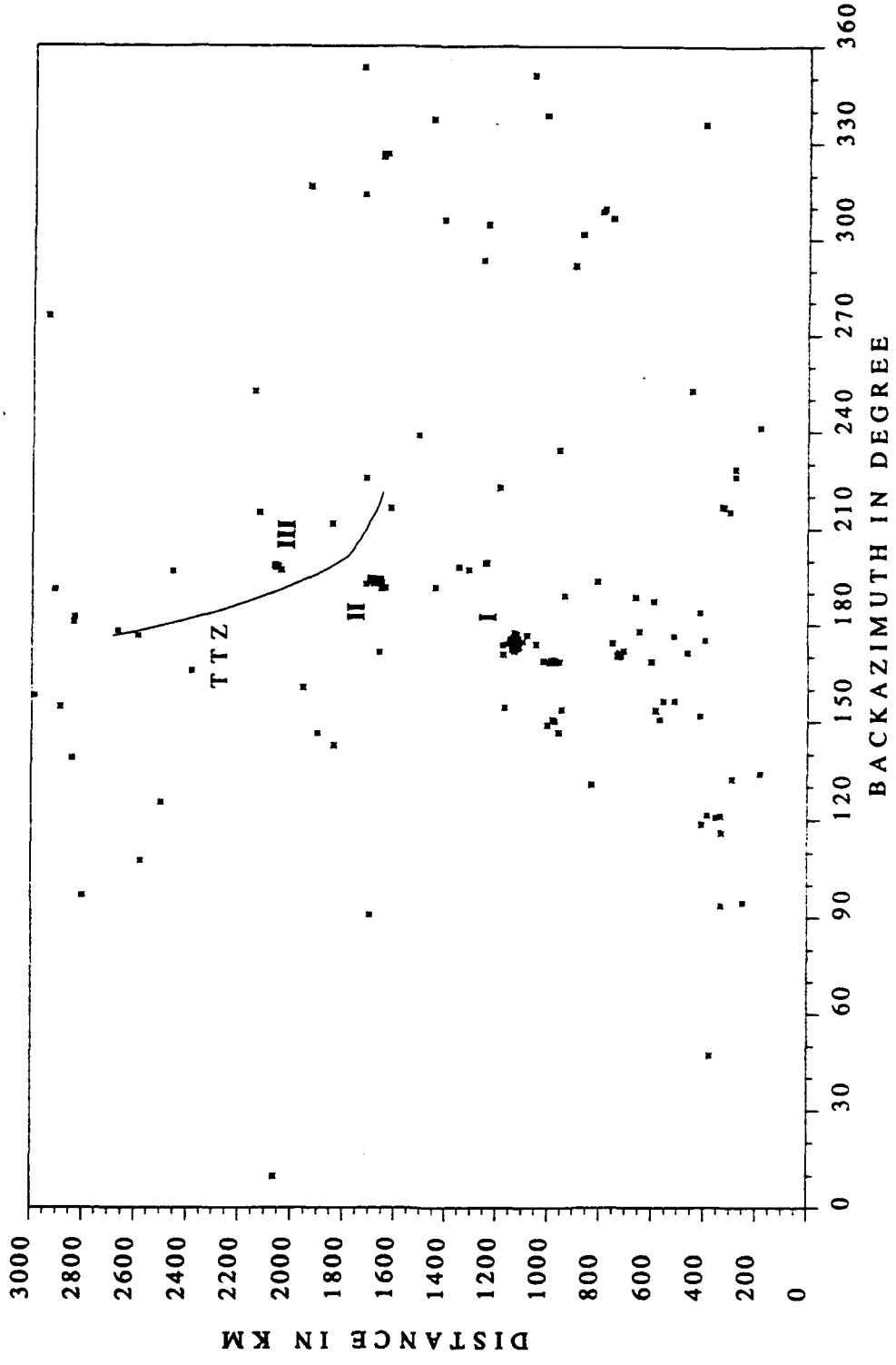
DISTANCE IN KM
3000
2800
2600
2400
2200
2000
1800
1600
1400
1200
1000
800
600
400
200
0
BACKAZIMUTH IN DEGREE
0
30
60
90
120
150
180
210
240
270
300
330
360
TTZ
I
II
III

b

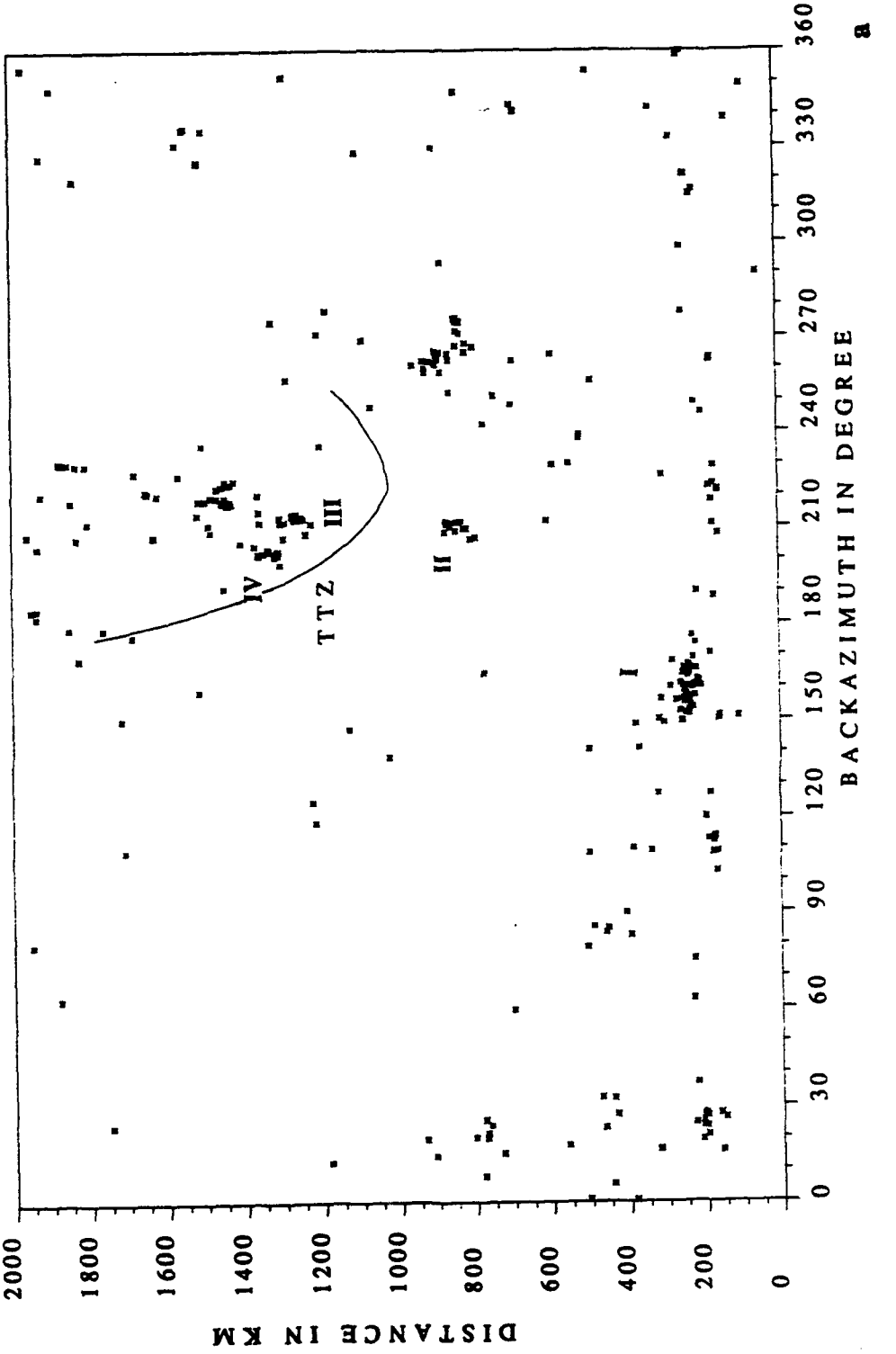

Fig. 2-7: as Fig. 2-4, but for the FINESA array. (165 of 323 events were detected)

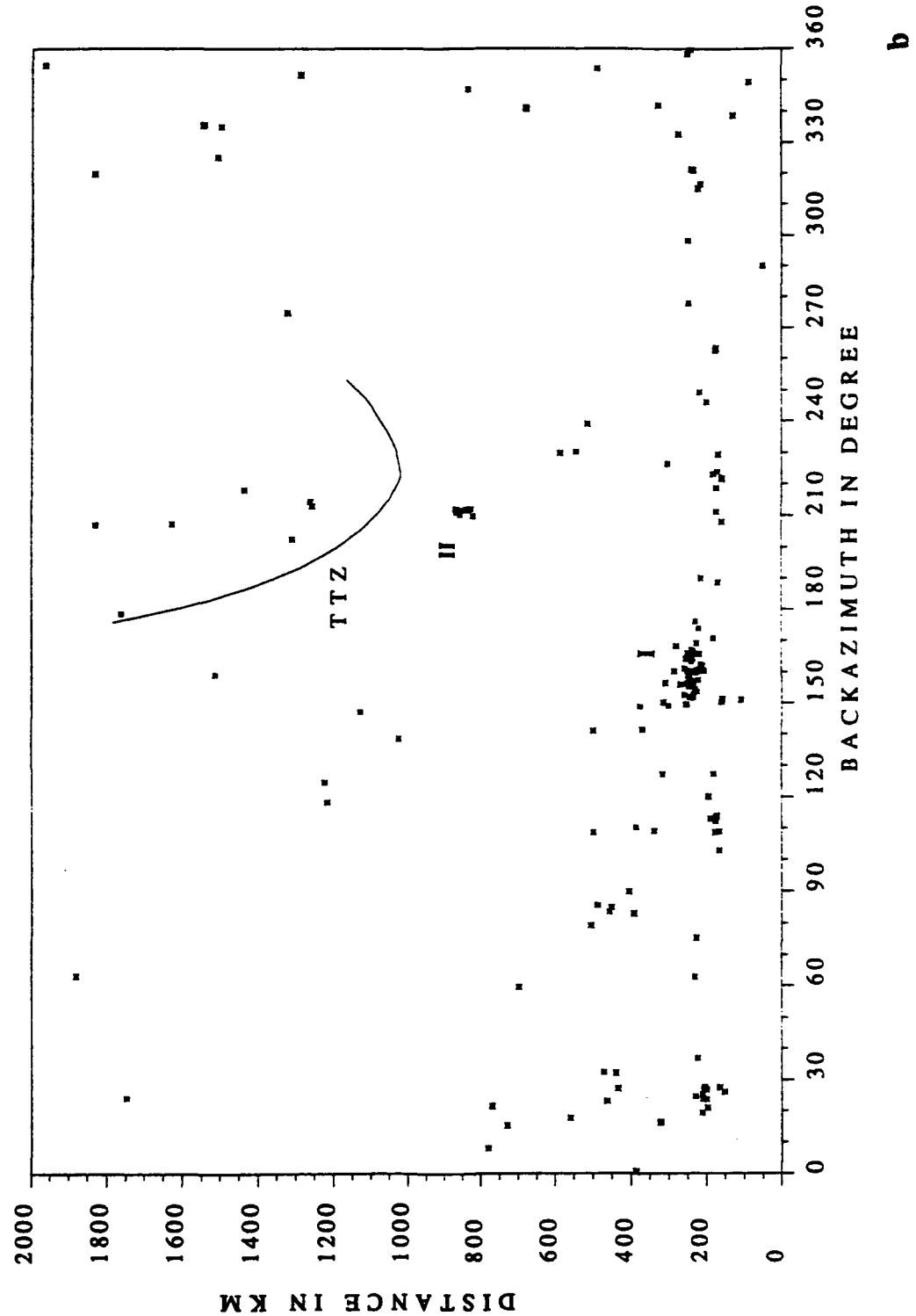
DISTANCE IN KM
2000
1800
1600
1400
1200
1000
800
600
400
200
0
BACKAZIMUTH IN DEGREE
0
30
60
90
120
150
180
210
240
270
300
330
360
TTZ
II
I

b

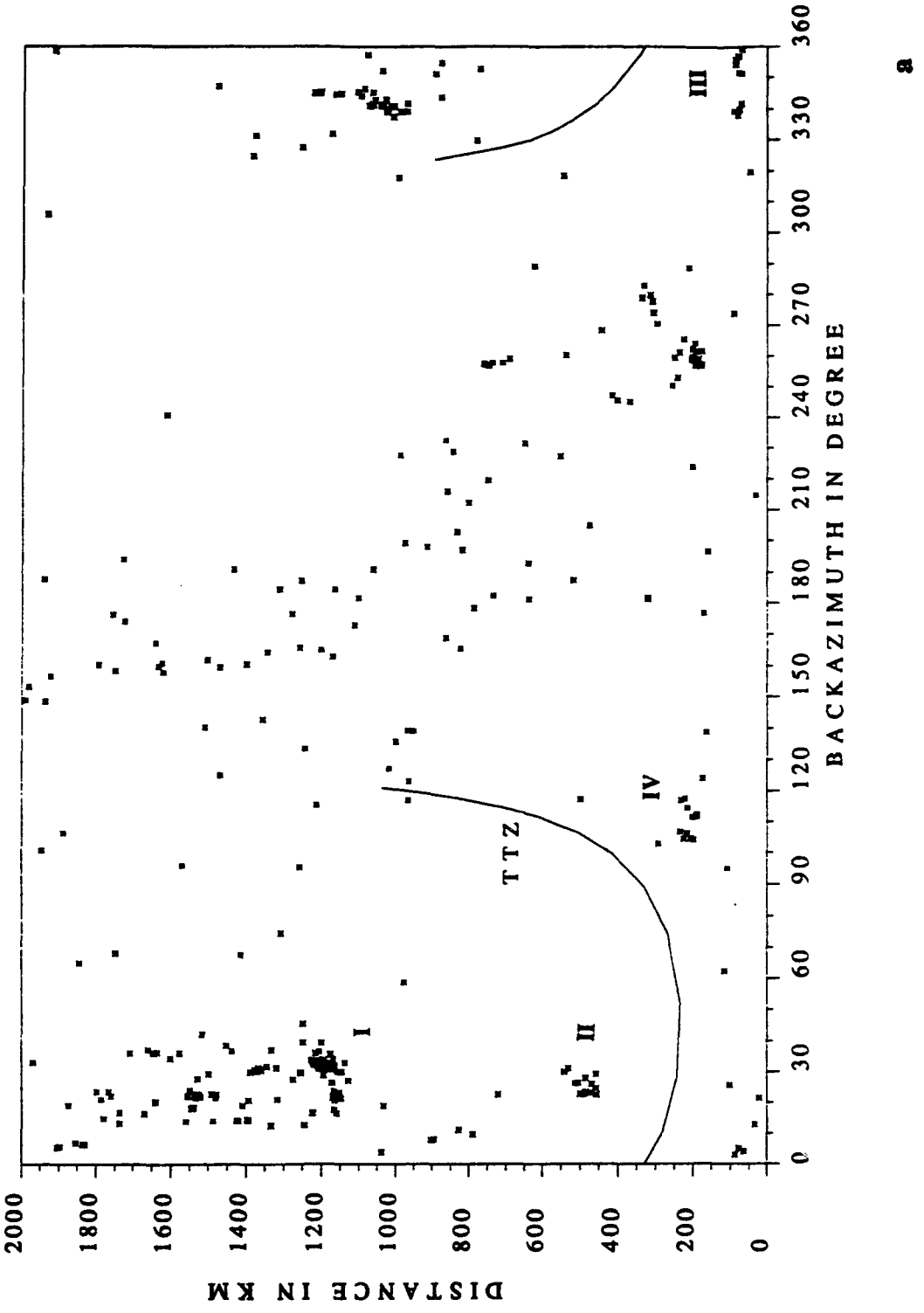

Fig. 2-8: as Fig. 2-4, but for station KSP. (60 of 347 events were detected)

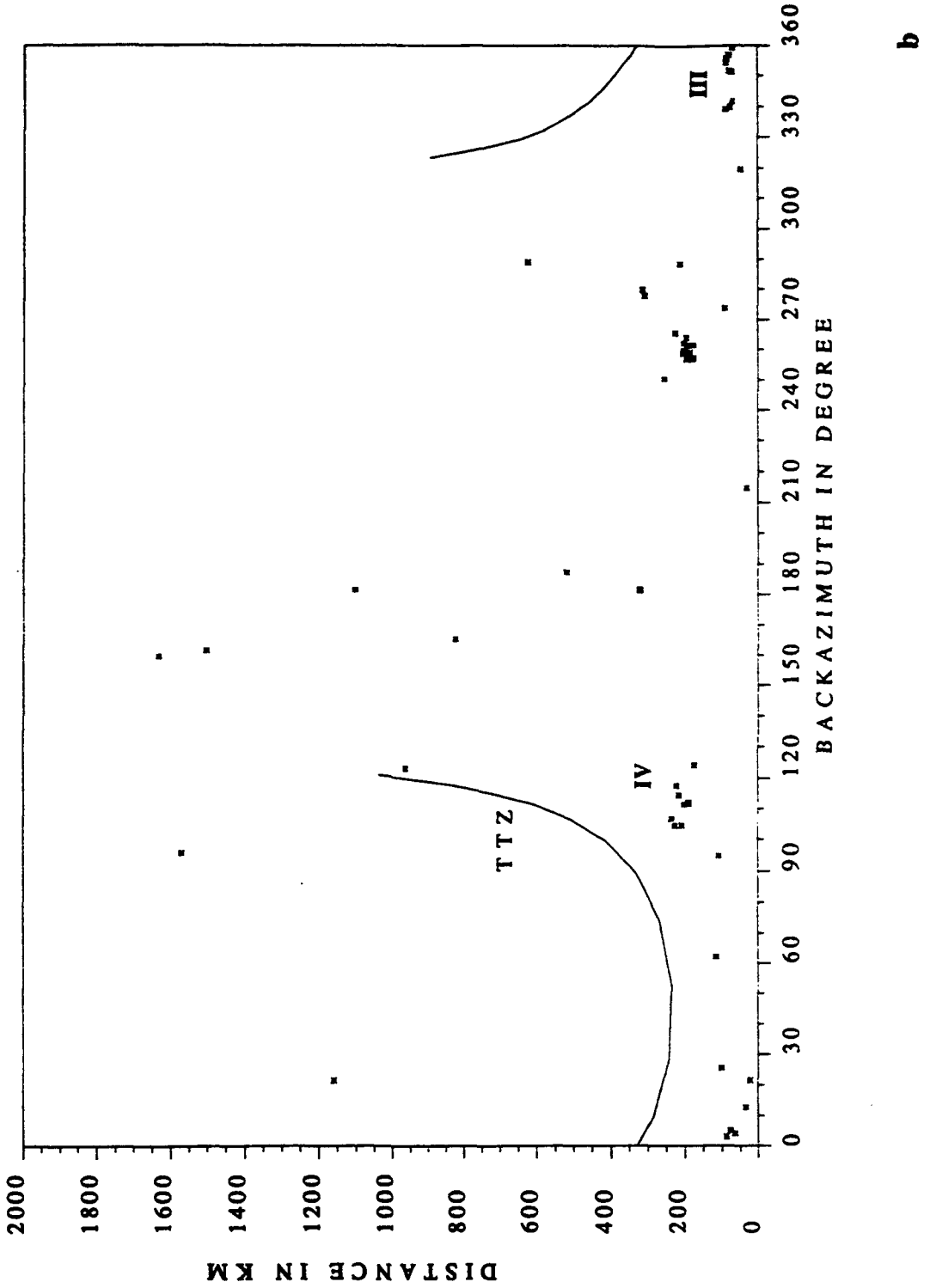
DISTANCE IN KM
2000
1800
1600
1400
1200
1000
800
600
400
200
0
0
30
60
90
120
150
180
210
240
270
300
330
360
BACKAZIMUTH IN DEGREE
T T Z
IV
III

b

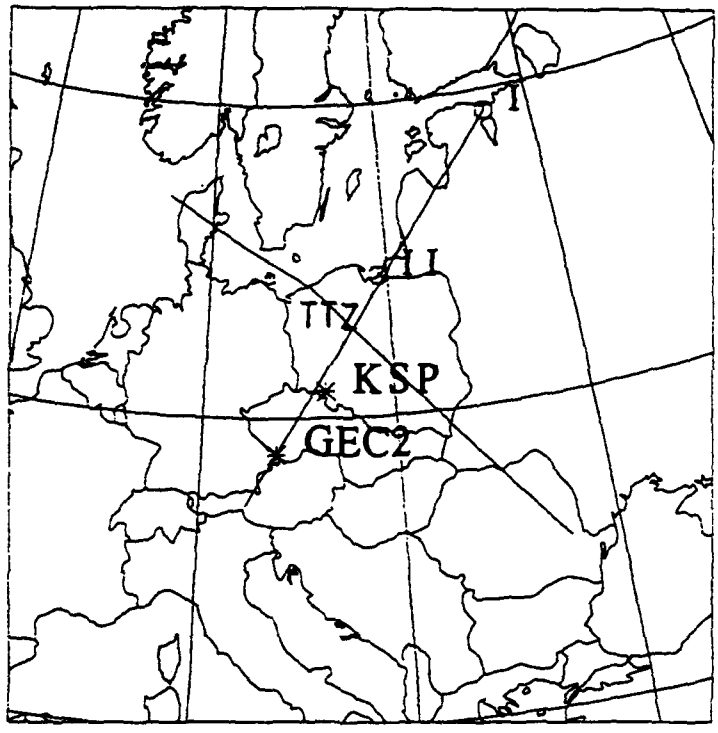

Fig. 2-9: The modelled profile - perpendicular to the TTZ and parallel to the International Profile VII - with source regions I and II and the positions of GERESS (here called with its key station GEC2) and KSP.

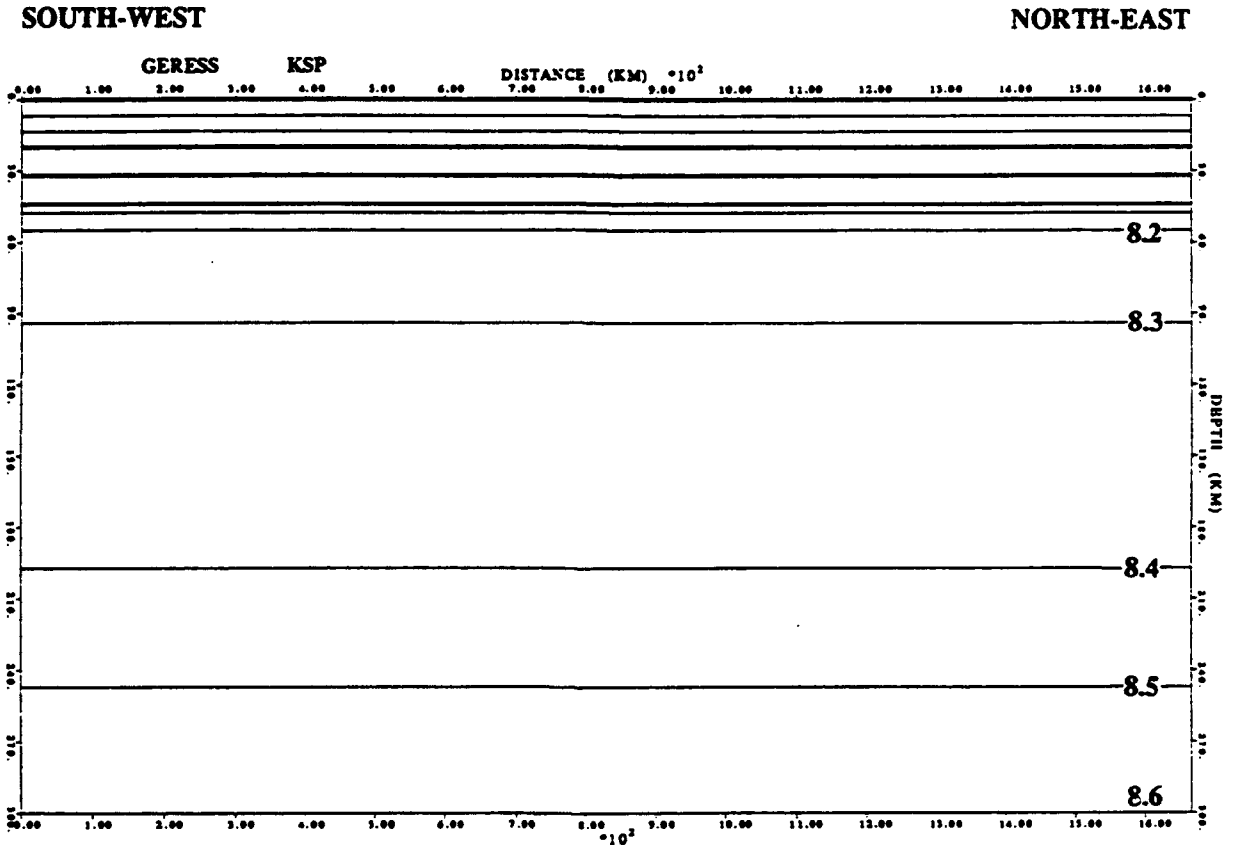

Fig. 2-10: Isolines of the P-velocitie (km/s) in the 1D model of the East European Platform MUMEP (after Grad, 1987). Thick lines represent first order discontinuities in the model.

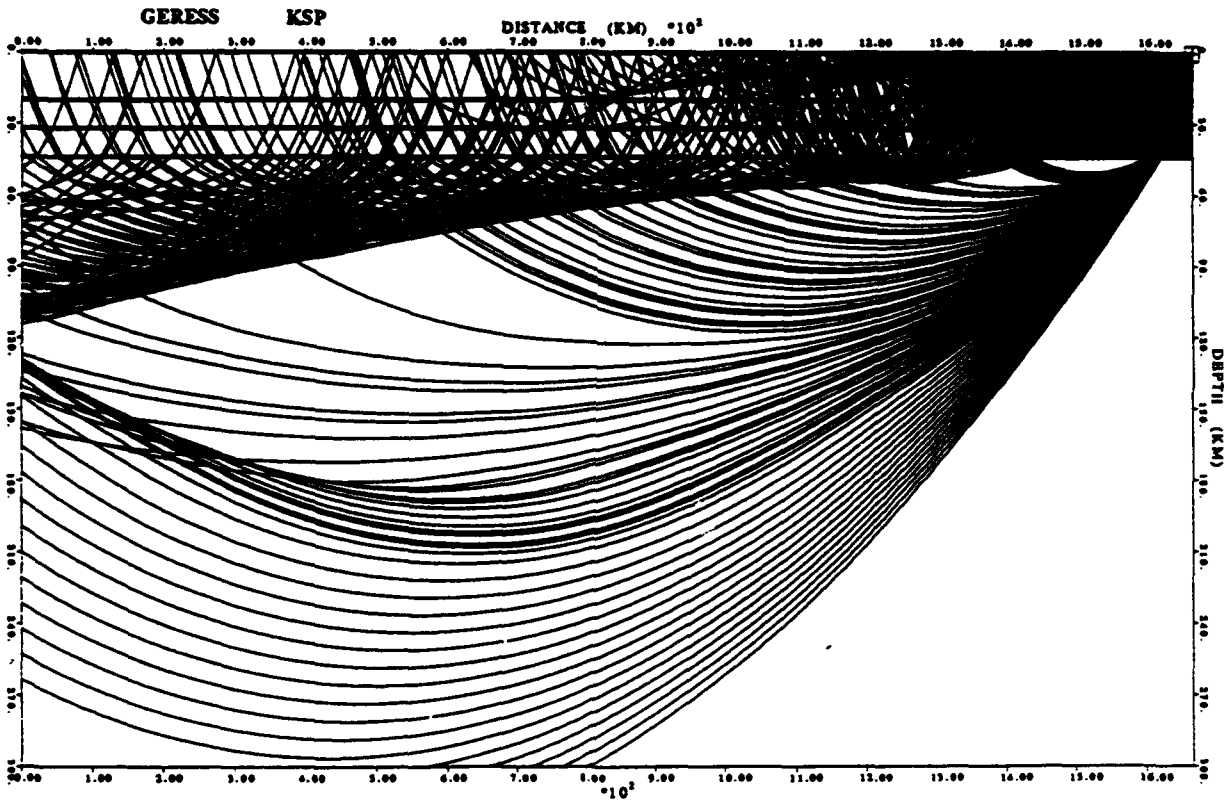

Fig. 2-11: Rays of all calculated phases in the ID model. The source was assumed to be at the right end of the profile at source region I in the Estonia-Russia border region (1667 km). The positions of the station KSP and the GERESS-array are marked.

Fig. 2-12: Theoretical seismograms for the laterally homogeneous model calculated with the Gaussian beam method. The seismograms had been normalised with the maximum amplitude of the trace in 700 km. The seismogram section is reduced with 8.1 km/s.

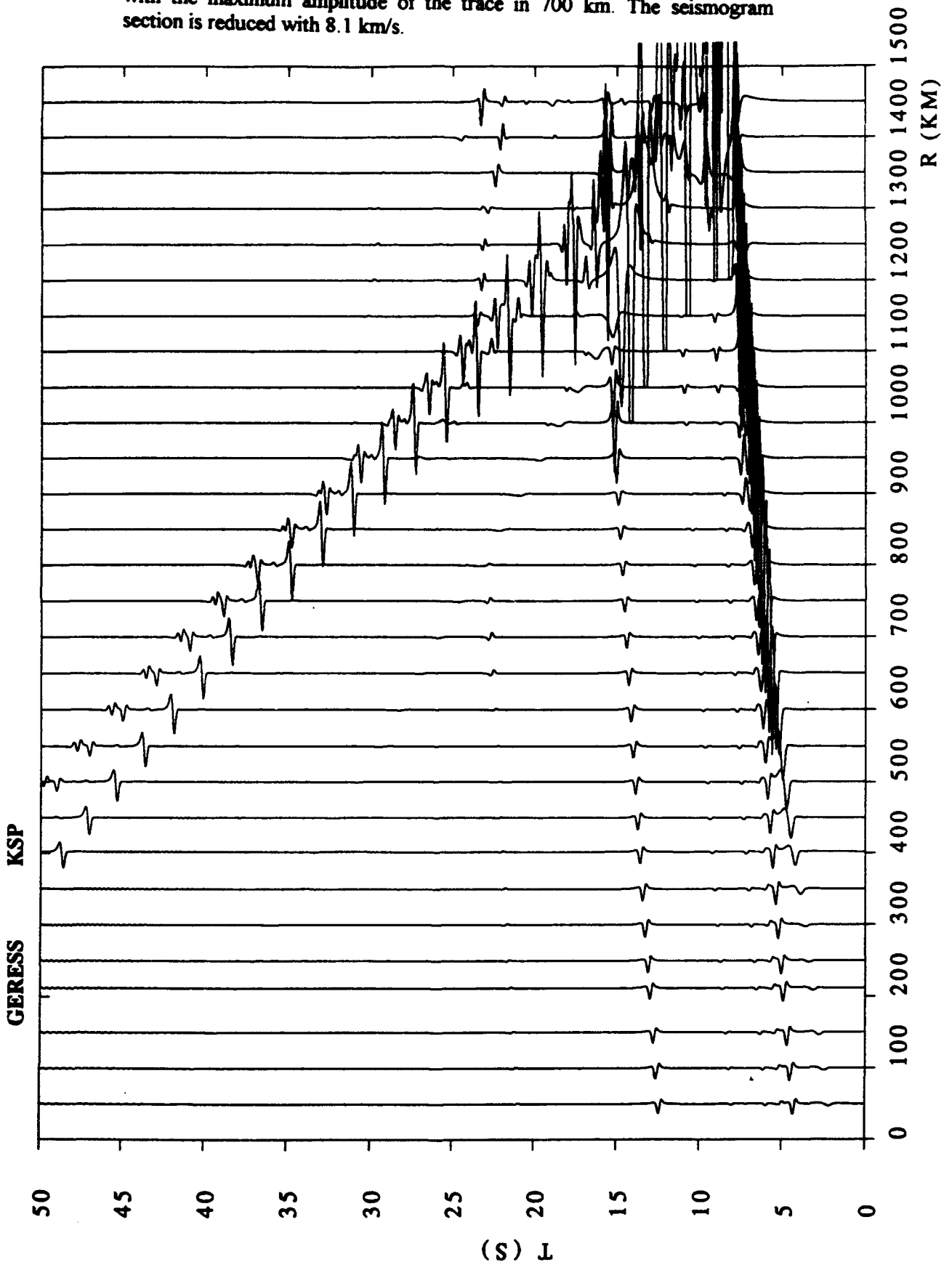

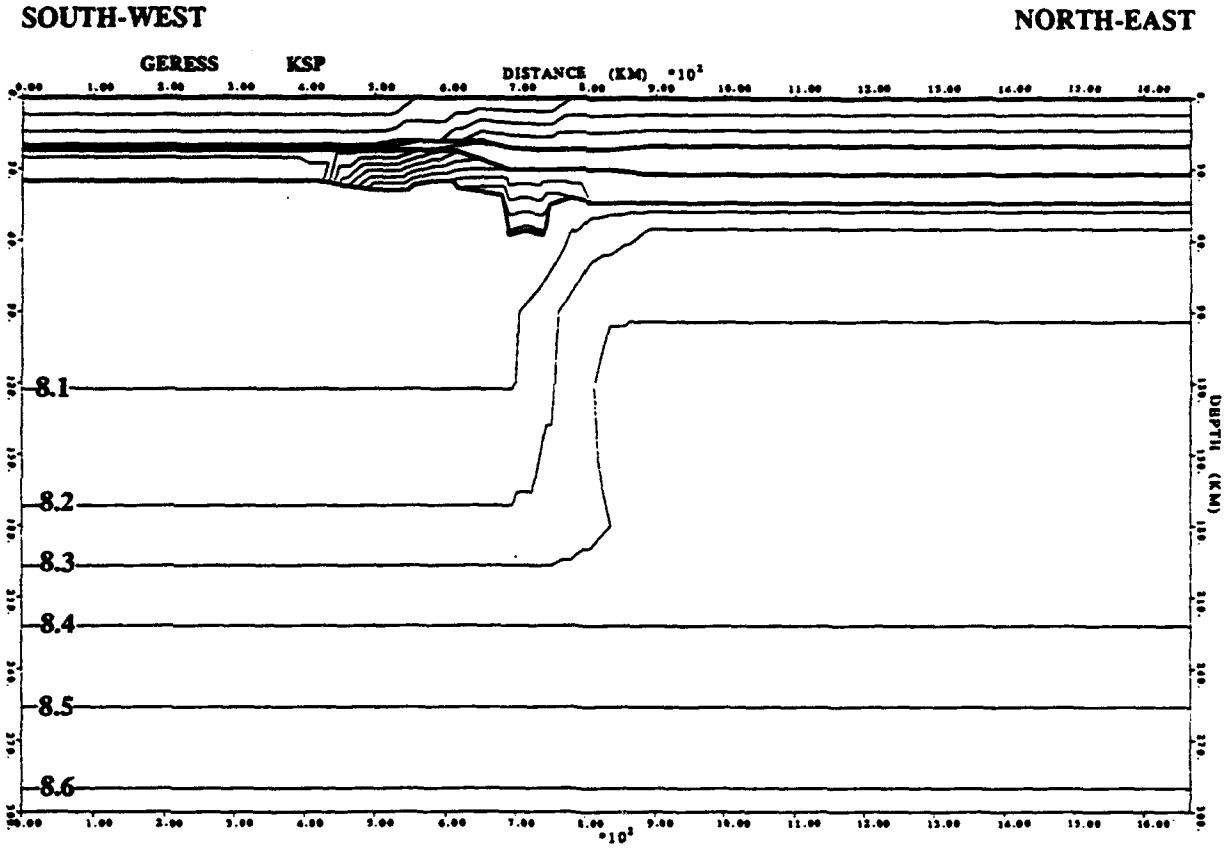

Fig. 2-13: The P-velocity structure of the first laterally heterogeneous model.

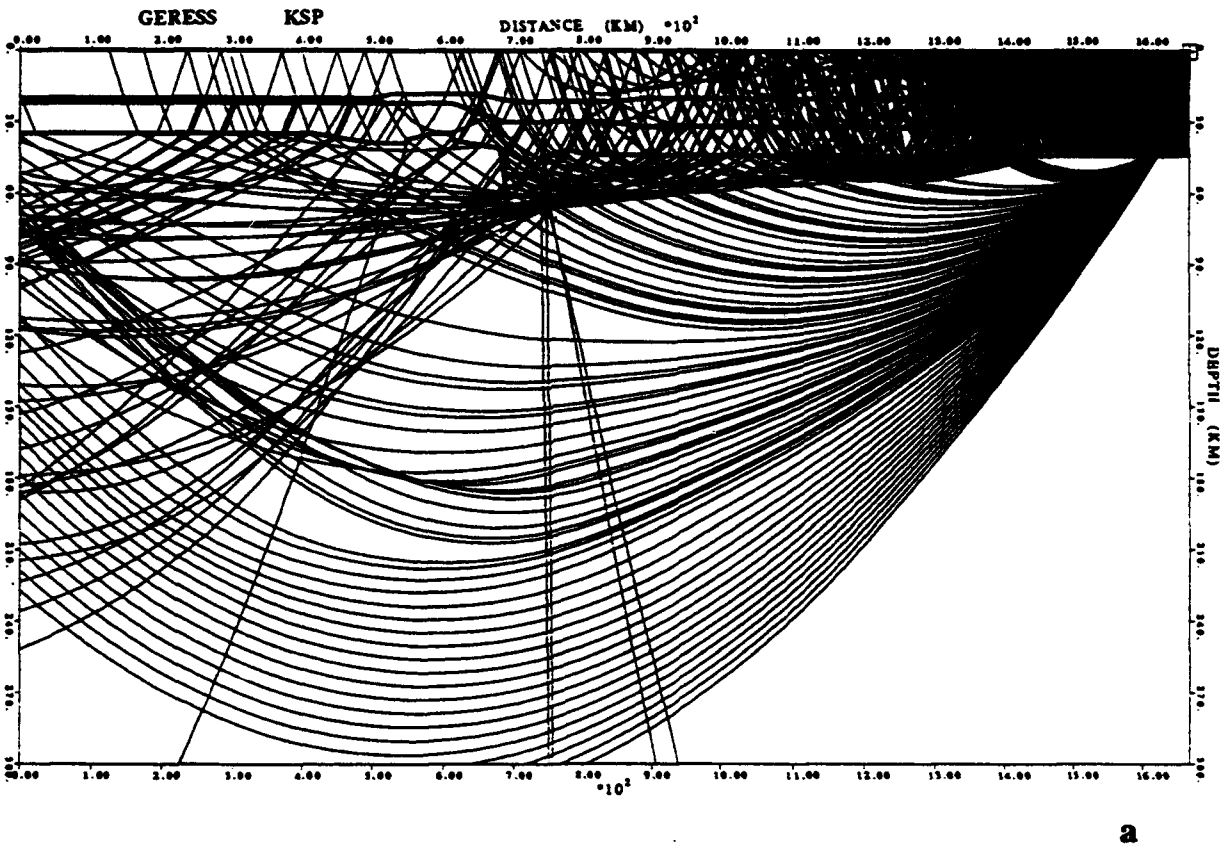

a

Fig. 2-14: a) as Fig. 2-11, but for the first laterally heterogeneous model. b) as before, but for a source at source region II in the Bay of Gdańsk (959 km).

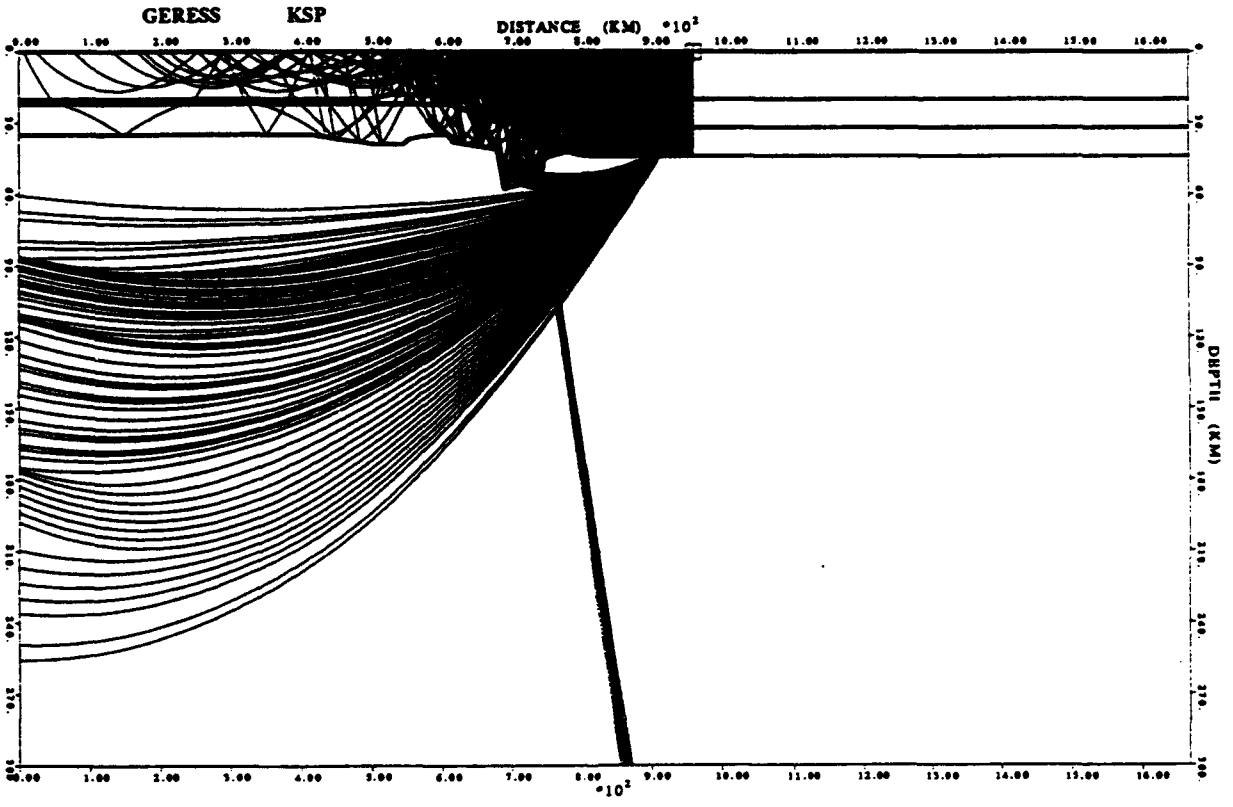

b

Fig. 2-15: a) Theoretical seismograms calculated with the Gaussian beam method as in Fig. 2-12 but for the first TTZ model (Fig. 2-13). b) as before, but for an event at source region II.

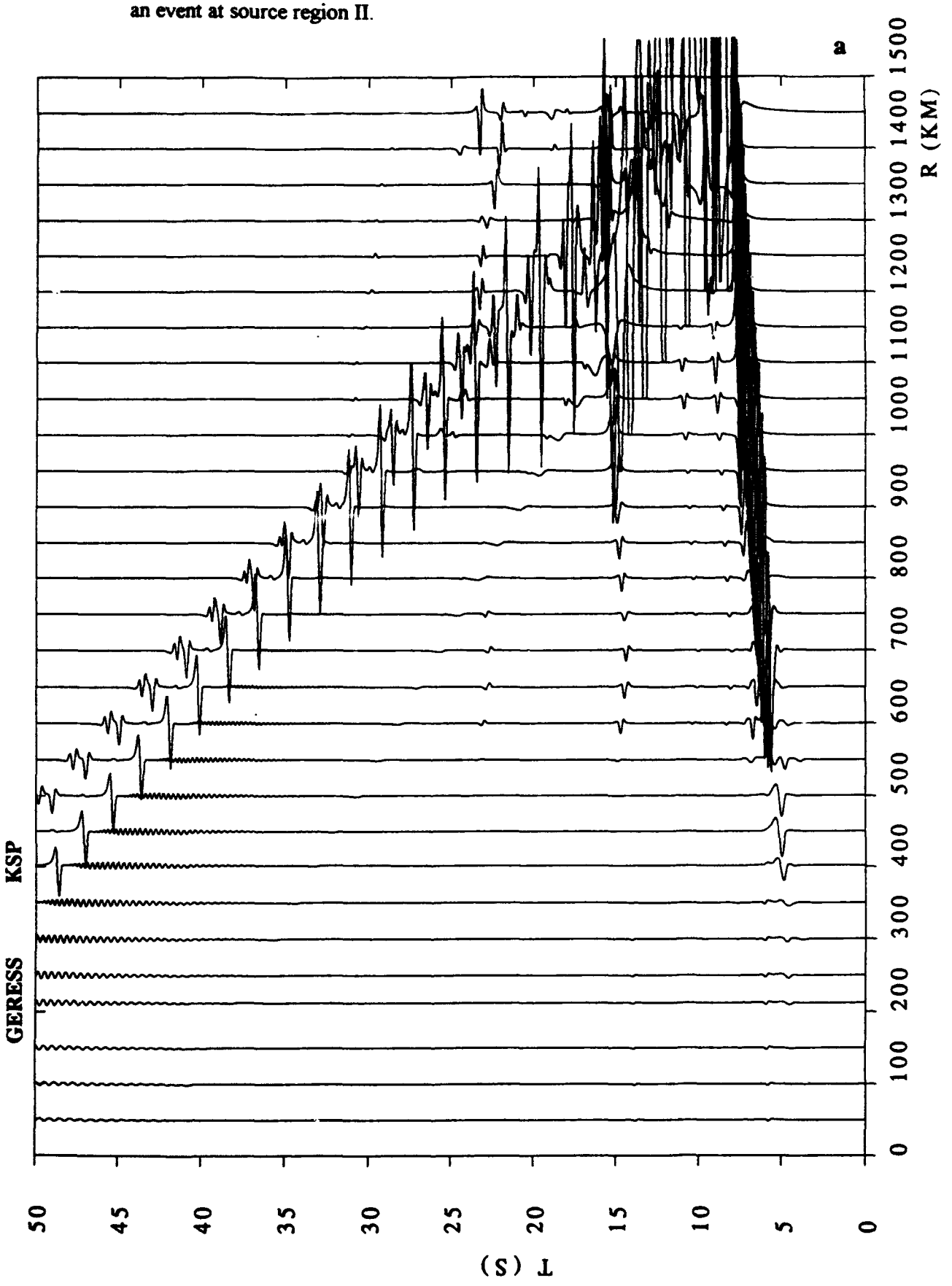

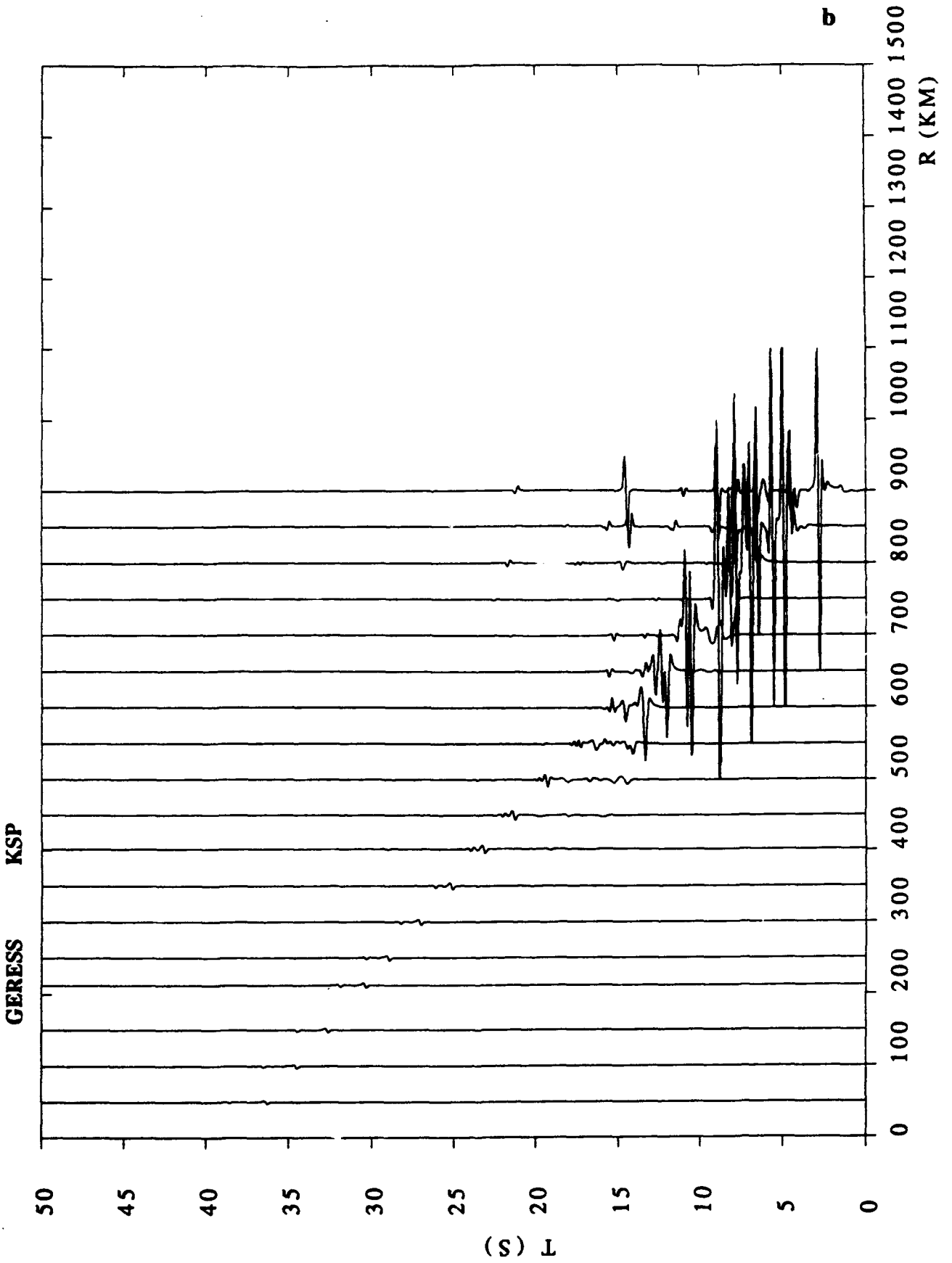
b
GERESS KSP
R (KM)
0 100 200 300 400 500 600 700 800 900 1000 1100 1200 1300 1400 1500
T (S)
0 5 10 15 20 25 30 35 40 45 50

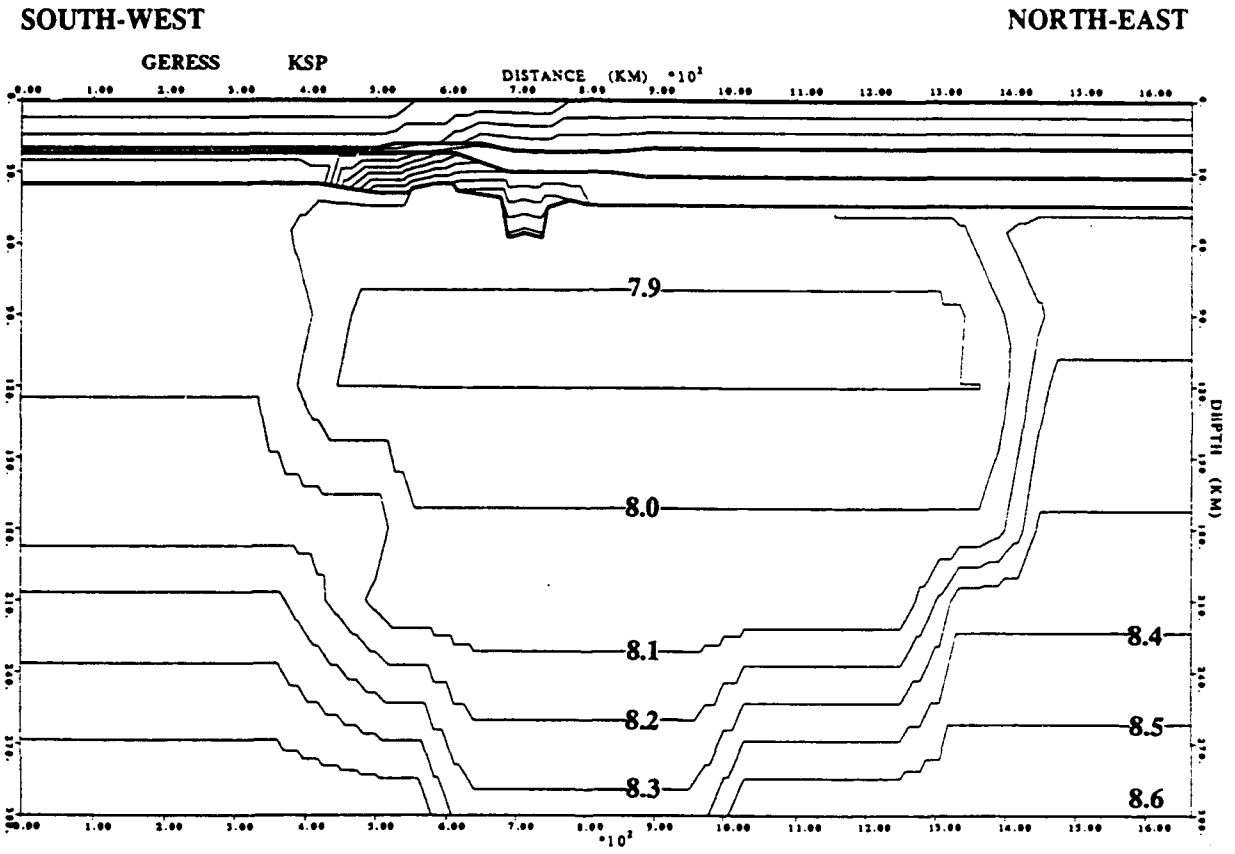

Fig. 2-16: as Fig. 2-13, but for the final P-velocity model of the TTZ and the uppermost mantle beyond the TTZ.

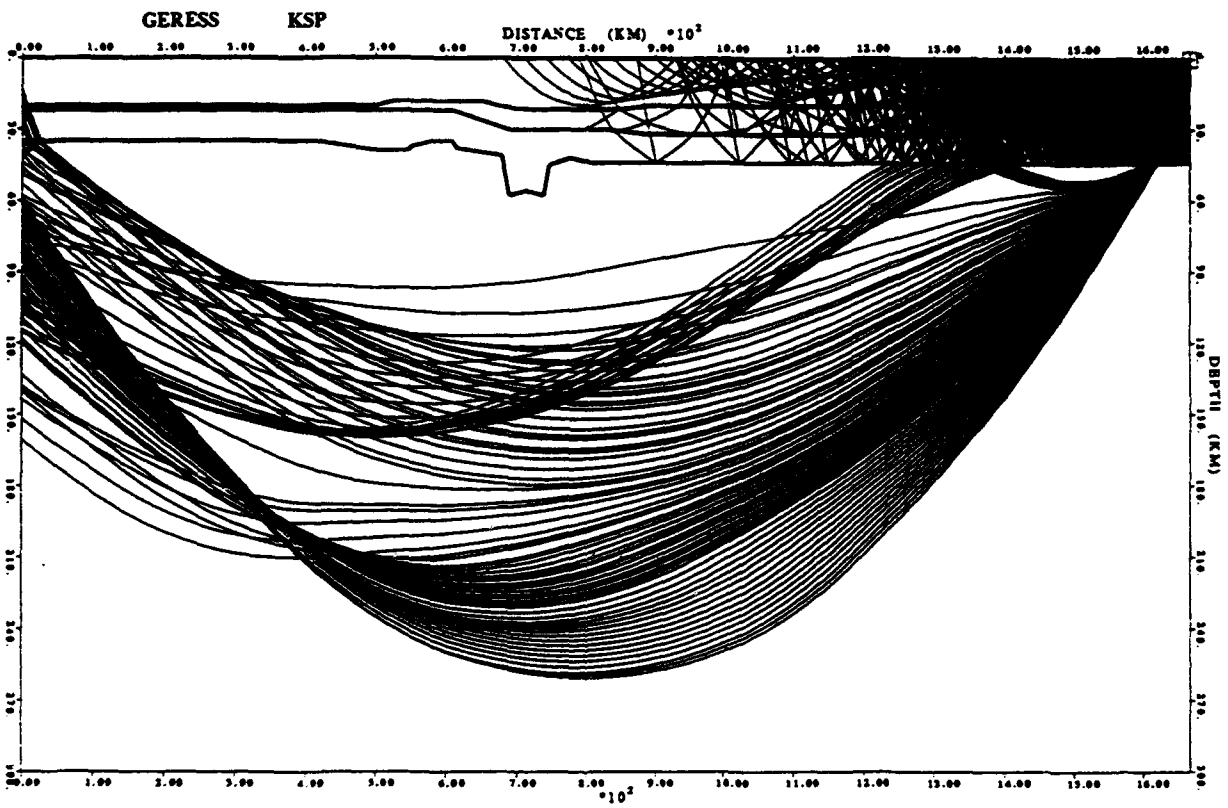

a

Fig. 2-17: as Fig. 2-14, but for the model of Fig. 2-16.

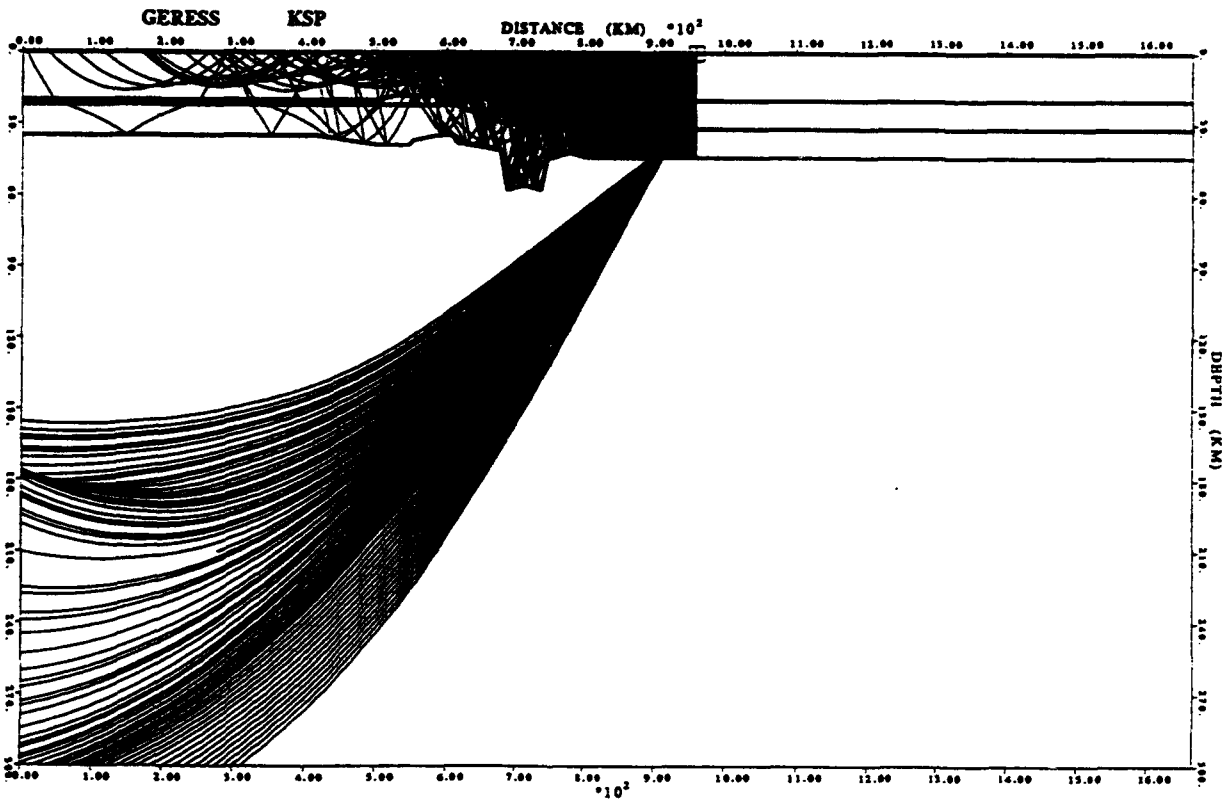

b

Fig. 2-18: as Fig. 2-15, but for the model of Fig. 2-16.

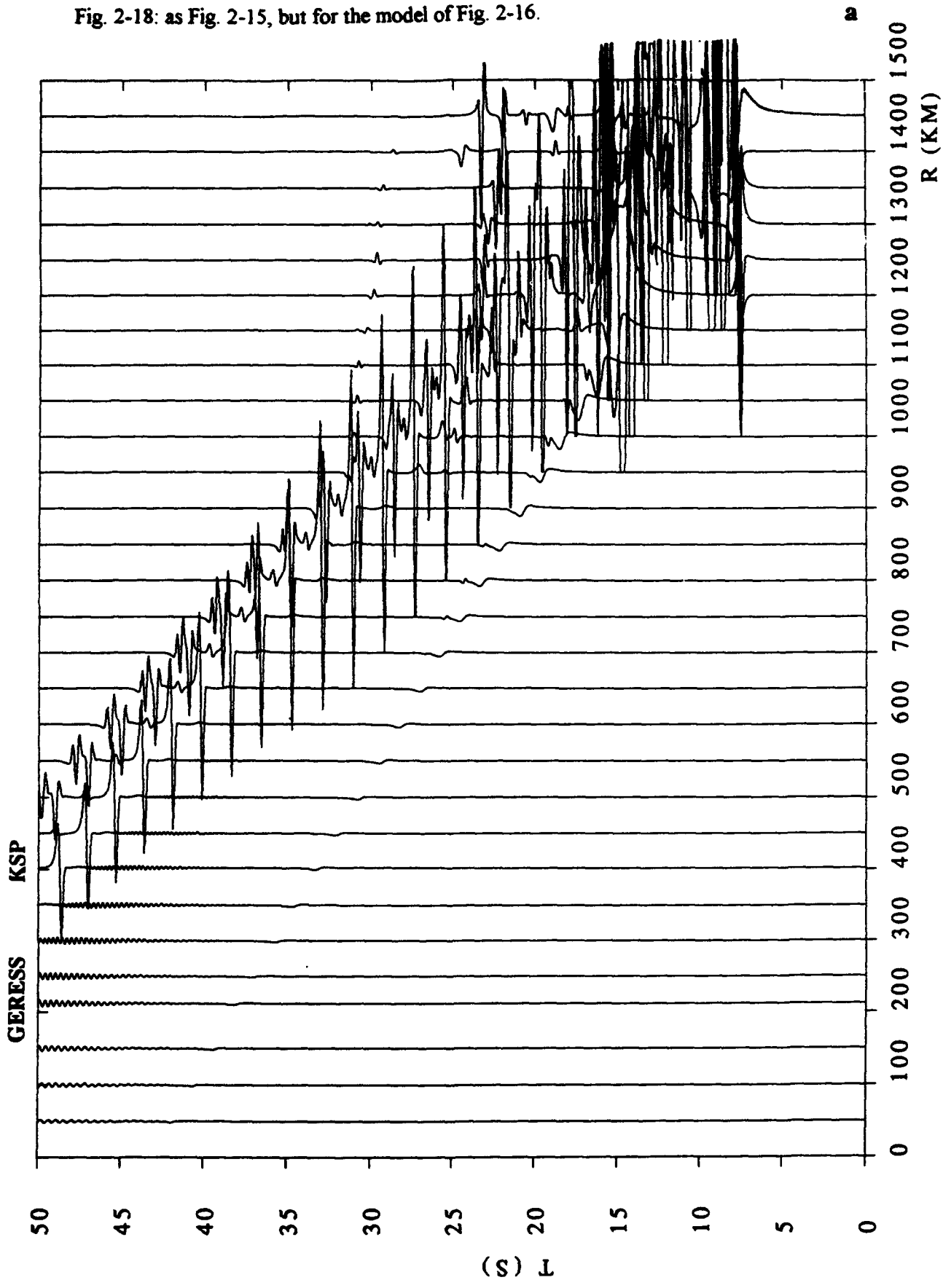

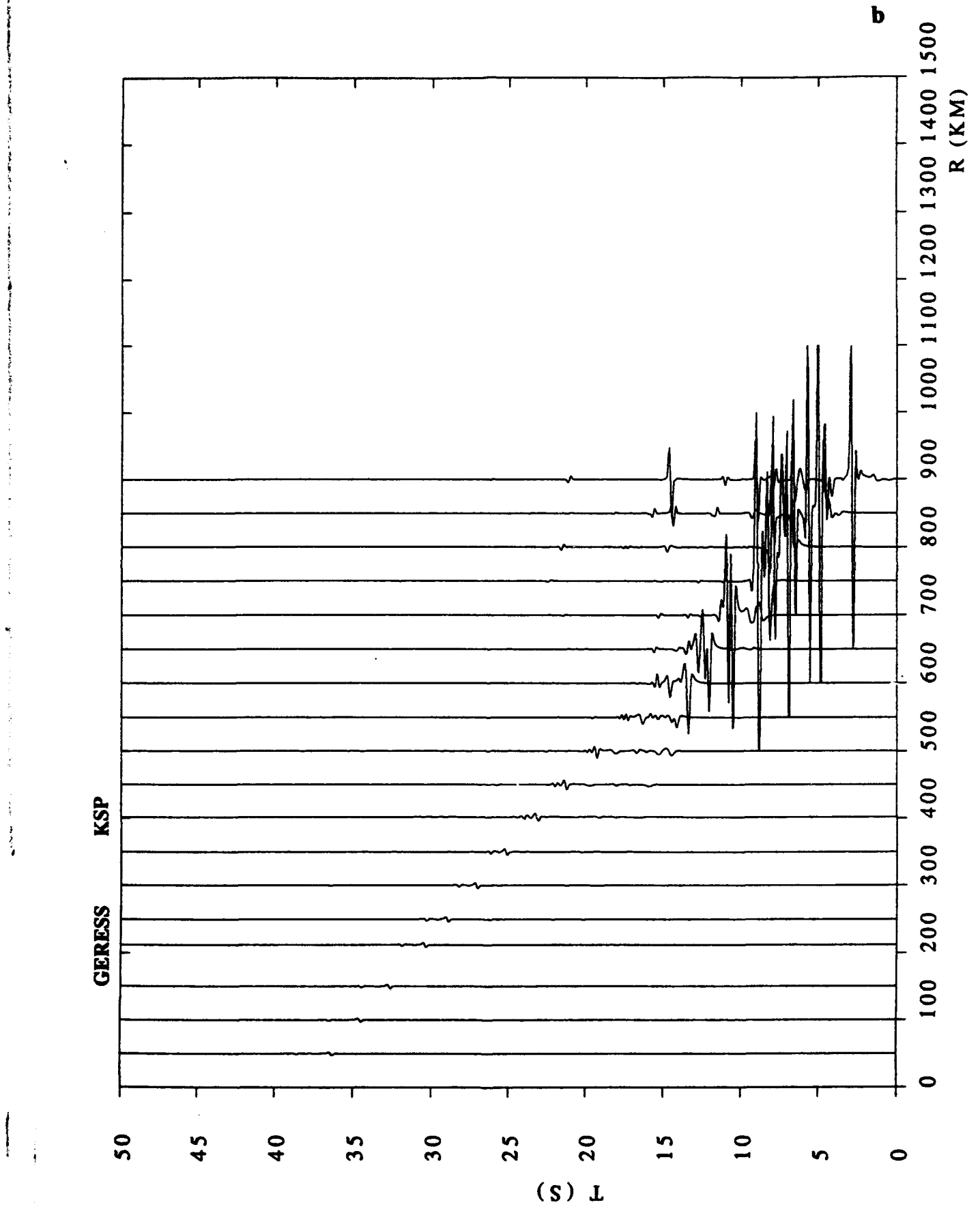
b
GERESS
KSP
0
100
200
300
400
500
600
700
800
900
1000
1100
1200
1300
1400
1500
R (KM)
50
45
40
35
30
25
20
15
10
5
0
T (S)

3. SIGNIFICANT AZIMUTH AND SLOWNESS DEVIATIONS FROM THE GERESS REGIONAL ARRAY*

Götz H.R. Bokelmann

3.0 Abstract

How accurate are horizontal slownesses determined from small arrays such as the German Experimental Seismic Array System (GERESS)? Travel times at GERESS array stations can typically be fit by plane waves to within a hundredth of a second. Slowness uncertainties are about 0.5 s/°, while azimuthal uncertainties are about 2° for regional events and less than 5° for teleseismic nuclear events. Using a single regional array in Europe, events from Nevada and Tuamotu nuclear test regions can be easily distinguished. The uncertainties, however, require array topography (about 200 meters for GERESS) to be taken into account. Such a 3D array allows determination of the vertical slowness, which gives a local velocity of 5.2 km/second under the GERESS array.

Statistically significant deviations of slownesses and azimuths are observed using the GERESS array, although it is has an aperture of only 4 km. These effects should be taken into account in order to improve source localization procedures.

3.1 Introduction

Recently, two international seismological experiments were set up to test the performance of global seismological networks (GSETT-1 in 1984 and GSETT-2 in 1991). Due to the importance of such networks for nuclear verification, the objective focused on detection and location capabilities. The experiments comprised both single-stations as well as teleseismic and regional arrays. The GSETT-2 experiment (GSE/35/CRP/228, 1993) showed that particularly the arrays played a very important role. Without them only 911 events were defined out of otherwise 3715 events. While large teleseismic arrays exist for several decades, many small regional arrays were recently deployed, primarily for the objective of creating in-country installations for verification of nuclear tests. These regional arrays typically have array configurations on concentric circles motivated from antenna theory and apertures of just a few kilometers.

The prime feature of arrays is the capability of measuring components

*submitted to BSSA

of the slowness vector **p**, in addition to stabilized estimates of travel time and amplitude of an individual body wave phase. Each component p_i of this vector represents the reciprocal of the velocity $\frac{dT}{dx_i}$ in that particular direction x_i, hence the apparent velocity. The component $p_\parallel$ in the direction of the source-receiver great circle azimuth is generally called the "ray parameter" or simply the slowness. $p_\parallel$ has been extensively used in the past to infer 1D Earth structure, since it directly represents the reciprocal velocity at the turning point of a ray in a 1D medium with plane geometry. Modern arrays typically extend in two directions on the Earth's surface thereby allowing measurement of two horizontal slowness components p_x and p_y or alternatively $p_\parallel$ and backazimuth θ. Their deviations from predictions of a reference velocity model are typically represented as mislocation diagrams (f.e. Davies and Sheppard, 1973 and Berteussen, 1975 for LASA; Okal and Kuster, 1975 for FPSN; Faber et al., 1986 and Krüger and Weber, 1992 for GRF; Schweitzer, pers.comm. for GERESS). While $p_\parallel$ has direct implications on 1D Earth structure, the azimuthal deviation gives further clues, namely about lateral heterogeneity. For first-arriving phases azimuthal deviations of several degrees from the reference model are typical for most arrays. In qualitative studies such anomalous effects were ascribed to lateral heterogeneity in the lower mantle (Davies and Sheppard, 1973; Weichert, 1972), the crust and upper mantle (Berteussen, 1975; Faber et al., 1986; Okal and Kuster, 1975) or a sedimentary layer under the respective array (Krüger and Weber, 1992).

Clearly, arrays are very important for the primary need of event detection and location; on the other hand, they also have potential from an Earth-structure point of view. However, till very recently there were no attempts to use azimuthal and slowness information as input data in a formal inversion. While this is possible in principle (Hu and Menke, 1992; Bokelmann, 1993), it should be studied whether slowness and azimuth observations of the respective arrays are accurate enough to be used as input data and whether they contain information about the propagation medium at all. While this is often the case for larger arrays we are particularly interested in *small arrays*, since large amounts of such data have recently become available through a number of regional arrays, which also participated in the GSETT-2 experiment. We will see below that slowness $p_\parallel$ and azimuth θ can in fact be measured accurately enough to make small arrays important contributors to global location procedures. In addition, significant deviations from reference model parameters are observed suggesting that these data can and should be used in 3D inversions to improve regional and global Earth models.

3.2 The GERESS Array

The GERman Experimental Seismic System GERESS (Harjes, 1990), shown in figure 3-1, is a regional arrays with aperture of about 4 km consist-

ing of 25 stations with 1 Hz vertical short-period instruments sampled at 40 Hz (solid circles), which are used in this paper, and a number of shortperiod and broadband 3-component instruments. The array is located in Eastern Bavaria, Germany, in a hilly region on granitic outcrop of the Bohemian massive. Topographic variation across the array of about 200 meters is shown by contour lines spaced at 25 meters, while the number after the station name gives elevation of the instrument (located in vault) relative to 1000 meters, the first solid contour. Also for the GERESS array, azimuthal deviations of first-arriving phases of several degrees are typical. We will see below that topography across the GERESS array accounts for some but not all of these azimuthal deviations. The remnant is due to lateral heterogeneity.

The standard method for estimating slowness and azimuth from array waveforms is the wavenumber spectrum technique, which is also used in automatic procedures (Fyen, 1987, Harjes et al., 1993). While this method uses the full waveform information on the array channels explicitly, $p_{\|}$ and θ can also be extracted from travel times by fitting a plane wavefront. Using that procedure, standard errors of $p_{\|}$ and θ follow directly from the least-squares approach for travel time fitting, while errors for the wavenumber spectrum technique essentially require a known noise correlation. Out of that reason we use travel times here. However, uncertainties of both methods should in principle be of comparable size.

Travel times are determined from waveforms by choosing either a fixed position in the waveform (onset, maximum, minimum, zero-crossing) or by correlating parts of the waveform (crosscorrelation, visual correlation). Practical aspects of extracting travel times are discussed in Weichert (1975). Compared to the crosscorrelation method, visual correlation offers added flexibility in choosing window lengths. We use that method for the first few seconds of the waveform in raw waveform data. Formal errors from plane-wave fitting suggests that the relative lag in waveforms of different stations can be determined to subsample accuracy, e.g. with resampling the data. This is consistent with uncertainties of crosscorrelation delays (Bokelmann, 1992) which can reach values of a tenth of a sample interval depending on the signal-to-noise ratio. Here the sampling rate is not the limiting factor, but waveform distortions, f.e. from noise contamination or from physical effects affecting waveforms such as scattering from near-receiver heterogeneity.

TABLE 1: Standard Errors of Slowness Estimates for Selected Arrays

Array	Country	Aperture	σ_p	Reference
SCARLET	USA	480km	0.02s/deg	Walck&Minster 1979
TFSO	USA	300km	0.1s/deg	Johnson 1969
LASA	USA	250km	0.1s/deg	Chinnery&Toksöz 1967
GRF	Germany	100km	-	Faber et al 1986
YKA	Canada	25km	0.1s/deg	Weichert 1972
YKA	Canada	25km	0.05s/deg	Weichert 1975
GERESS	Germany	4km	0.5s/deg	average value for this study

Table 1 gives typical slowness errors extracted from teleseismic (large, medium) and regional (small) arrays. Larger arrays generally have smaller errors. Large aperture arrays SCARLET in California, TFSO in Arizona, LASA in Montana and GRF in Germany show error of 0.1 s/° or smaller. Table 1 also gives values for intermediate size (YKA) and small regional arrays (GERESS), which are larger. For YKA with an aperture of about 20 km the slowness error is still comparable to ones of large arrays (Weichert, 1972), while GERESS, a regional array with aperture of 4 km, gives errors of about 0.5 s/° as an average value for regional and teleseismic events in this study. Azimuthal uncertainties are about 2° for regional events and about 5° for teleseismic events. Even though this uncertainty is larger than for large arrays, it is small enough to observe significant array effects. Of course, array size is not the only factor affecting the slowness error. Since waveform coherence decreases with distance, smaller arrays have the advantage of strong waveform coherence. In fact, both GERESS and YKA perform much better than expected from theoretical resolution arguments, where σ_p should be proportional to $(Aperture)^{-1}$; for GERESS by a factor of 3, for YKA even a factor of 5.

Large arrays fight against the problem of incoherent waveforms, but also of variation in slowness across the array (Burdick and Powell, 1980). They effectively average over resulting travel time curves and potential triplications (Wright, 1981). Often, namely in inversions for Earth's structure, this averaging is not desired. In the view of structural studies it is clearly an important question which accuracy smaller arrays can reach, particularly ones with diameters of just a few kilometers, which avoid this averaging. At the same time the averaging character of large arrays explains why large arrays have been very useful for source localization in the past. In fact, Burdick and Powell (1980) show that for the large SCARLET array most event azimuths and slownesses closely coincide with predicted values. Smaller arrays, on the other hand, may require calibration using observed array mislocations.

Polarizations from three-component data can also be used. However, those may be affected by anisotropy and the free surface. Errors are typically larger than those from array data (GSE/35/CRP/228, 1993). In comparison with a number of array determined slownesses and azimuths (North, pers.comm.),

values from three-component instruments were typically 4 times larger.

As opposed to such errors, we also have source location errors, for example from the GSETT-2 experiment, where differences between array quantities (azimuth and slowness) and predicted quantities using known or estimated source locations are computed. North (pers.comm.) reported slownesses for events during the GSETT-2 experiment and gave histograms, which can be characterized by slowness standard deviations of about 0.5 s/° for YKA, HFS and GRF and nearly 2 s/° for GERESS. These values are larger by a factor of 4 than the errors from table 1, one reason for the discrepancy being that these "source location" errors are also contain effects of lateral heterogeneity. In the following we will briefly state our method of slowness estimation and test the error estimates for consistency. We can then judge whether the array mislocation effects are significant and may give rise to the difference between the two types of error estimates.

3.3 Slowness Vector Components

We can write the travel time of a plane wave at the i-th station as

$$t_i = t_0 - \mathbf{p}\mathbf{r}_i \tag{1}$$

where $\mathbf{p}$ is the slowness vector (defined from receiver to source) and $\mathbf{r}_i$ the location vector for the i-th station. t_0 is the estimated time at the reference station. This is a "forward" problem $\mathbf{t} = \mathbf{A}\mathbf{x}$ with unknowns $\mathbf{x} = (t_0, p_x, p_y, p_z)^T$. Incorporating the vertical slowness p_z accounts for elevation differences of up to 200 meters across the 4 km aperture of GERESS. Using the singular value decomposition $\mathbf{A} = \mathbf{U}\mathbf{\Lambda}\mathbf{V}^T$, an estimate of the model vector is $\mathbf{x} = \mathbf{V}\mathbf{\Lambda}^{-1}\mathbf{U}^T\mathbf{t}$. The solution depends on the included number of singular values λ_j (diagonal elements of $\mathbf{\Lambda}$) included in the inversion. The fit to the data $\mathbf{t}$ is the better the more singular values are included. But at the same time features of the model (here the reference station travel time t_0 and the components of the slowness vector $\mathbf{p}$) are generated, which are unconstrained by the data. This is seen in the covariance matrix of the model

$$\mathbf{C} = \sigma_0{}^2\mathbf{V}\mathbf{\Lambda}^{-2}\mathbf{V}^T \tag{2}$$

for independent data normalized by the data standard deviations σ_0. Clearly, the variance or standard deviations may increase substantially if small singular values λ_j are incorporated. Model errors are not necessarily uncorrelated (see equation 2). We should keep in mind that marginal confidence regions are slightly optimistic (too small) in that case, although the effect is not large.

In our problem we can identify individual singular values with individual model parameters. For travel times of a typical teleseismic event (event 1 of table 3) we get the following 4 singular values and 4 right eigenvectors (columns of the matrix V)

Three of the four singular values are of the same order of magnitude, but the fourth is an order of magnitude smaller. The eigenvector for the smaller singular value describes essentially the influence of only the vertical slowness p_z on the data (bold print). This shows that p_z is more difficult to resolve than the other parameters, since it contributes an order of magnitude less to the data. Of course, this is expected since the elevation variations are an order of magnitude smaller than the array aperture.

Is it nevertheless reasonable to include p_z? A simple test is, whether we can recover the local velocity under the GERESS array from array observations of travel times which depends on vertical and horizontal slownesses through $c = \frac{1}{\sqrt{p_x{}^2+p_y{}^2+p_z{}^2}}$. Figure 3-2 shows a histogram of values for c for a number of different events and sets of travel times. The values scatter around the mean of 5.2 km/second with a standard deviation of 3.1 km/second. This is a reasonable value, since we expect to find an average velocity under the array. The waveform data in this paper (table 3), which will be extensively discussed later, contain regional and teleseismic events with apparent velocity ranging from 8 to 30 km/second. Although the two signal types differ substantially in apparent velocity, the distributions for c are indistinguishable. While this velocity represents some average over the velocities (fresh and weathered granite, gneiss) under the array, it is the value which should be used when converting from slowness $p_{\|}$ to incidence angle $arcsin(cp_{\|})$. It is curious to note that we can resolve the local velocity in principle from a single event, even without knowing the source location! Of course, such a direct determination of local velocity is possible only for a relatively small array like GERESS.

TABLE 2: Singular Values and Right Eigenvectors of **A**

Singular value nr:	1	2	3	4
Singular value size:	5.465	3.371	2.351	0.189
Eigenvector nr:	1	2	3	4
t_0	**-0.564**	0.363	**-0.734**	0.102
p_x	0.0272	**0.904**	**0.425**	-0.008
p_y	**-0.821**	-0.222	**0.524**	0.020
p_z	-0.075	0.025	-0.067	**-0.994**

Standard errors for p_z are one order of magnitude larger than ones for horizontal slownesses. Instead of deciding ad hoc whether to include p_z in the fitting we test the consistency of results in the next chapter. The standard errors depend on the errors in the data. From an internal consistency argument we obtain that these are on the order of 0.01 seconds.

TABLE 3: Events Used in this Study

Nr	Year, Day	Time	Latitude	Longitude	Mag.	Place	Phase	p_x/(s/deg)	p_y/(s/deg)
	Teleseismic Events:								
1	1990:285	17.30.00.08[1]	37.26N[1]	116.48W[1]	5.6[1]	Nevada	P	-3.06±0.49	3.78±0.45
2	1991:094	19.00.00.0[2]	37.296N[2]	116.313W[2]	5.6[2]	Nevada	P	-2.80±0.44	3.55±0.34
3	1991:257	19.00.00.05[2]	37.226N[2]	116.428W[2]	5.5[2]	Nevada	P	-2.70±0.26	3.49±0.22
4	1991:291	19.12.00.00[2]	37.063N[2]	116.045W[2]	5.2[2]	Nevada	P	-2.95±0.43	3.31±0.37
5	1990:153	17.29.59.0[1]	21.82S[1]	138.94W[1]	5.3[1]	Mururoa[3]	PKP	-2.09±0.56	2.18±0.43
6	1990:318	18.11.58.4[1]	22.20S[1]	138.84W[1]	5.6[1]	Fangataufa[3]	PKP	-2.16±0.35	2.45±0.27
7	1990:325	16.59.58.4[1]	21.90S[1]	138.98W[1]	5.4[1]	Mururoa[3]	PKP	-2.00±0.26	2.43±0.20
8	1991:138	17.14.58.53[2]	21.832S[2]	139.014W[2]	5.1[2]	Mururoa[3]	PKP	-1.76±0.23	2.56±0.21
9	1991:149	18.59.58.24[2]	22.256S[2]	138.794W[2]	5.5[2]	Fangataufa[3]	PKP	-1.98±0.29	2.67±0.25
10	1991:165	17.59.57.86[2]	21.944S[2]	138.988W[2]	5.2[2]	Mururoa[3]	PKP	-1.77±0.29	2.18±0.25
11	1991:196	18.09.58.33[2]	21.877S[2]	138.963W[2]	5.3[2]	Mururoa[3]	PKP	-1.61±0.38	2.02±0.45
	Regional Events:								
12	1991:059	15.29.40[4]	51.426N[4]	16.243E[4]	3.7[6]	Poland	Pn	6.07±0.46	11.65±0.34
13	1991:120	03.40.36[4]	51.409N[4]	16.264E[4]	3.4[5]	Poland	Pn	5.69±0.27	11.61±0.21
14	1991:143	19.42.54[4]	51.428N[4]	16.242E[4]	4.0[6]	Poland	Pn	5.08±0.64	10.49±0.63
15	1991:191	23.57.16[4]	51.424N[4]	16.217E[4]	3.3[7]	Poland	Pn	6.20±0.26	11.26±0.29
16	1991:222	05.23.48[4]	51.428N[4]	16.242E[4]	3.9[6]	Poland	Pn	6.55±0.60	11.22±0.53
17	1991:252	18.36.57[4]	51.414N[4]	16.220E[4]	-	Poland	Pn	6.36±0.24	10.99±0.21
18	1991:327	01.06.20[4]	51.428N[4]	16.243E[4]	3.9[7]	Poland	Pn	6.72±0.40	11.14±0.29

[1] ISC (mb), [2] PDE (mb), [3] DSIR, [4] POL, [5] KRA (ml), [6] VKA (ml), [7] GRF (ml).

Above we described how to obtain standard errors (marginal confidence regions). We test these by comparing results for events from identical source regions, both for teleseismic and regional data. In this fashion we can separate random fluctuations in the slowness components from systematic biases due to lateral heterogeneity along the ray path.

Figure 3-3 shows waveform data for event 6 of table 3, a French nuclear explosion on Fangataufa on the Tuamotu Archipelago, South Pacific. At

145° distance the bc branch of PKP is the first-arriving phase followed by the ab and the df branch within one second. Note the high spatial coherence, in particular of the first two seconds of the waveform. Using the first second of the waveform, correlation methods reach travel time accuracies well below one sample. For this event the effective data error is 0.01 seconds compared with a sampling interval of 0.25 seconds; the resulting uncertainty for $p_{\|}$ is 0.38 s/° at 1 standard deviation.

Slowness estimates shown in the following use travel times obtained using the RONAPP software package (Fyen, 1987). Events 1 through 4 in table 3 are US nuclear tests detonated in Southern Nevada, whereas events 5 through 11 are French tests from the South Pacific like the one shown in figure 3-3. Slowness components p_x and p_y are shown in figure 3-4a for the two regions with individual error bars giving one standard deviation. These result from an inversion for the 4 parameters (t_0, p_x, p_y, p_z) thereby accounting for array topography. Note that for each region the (p_x, p_y)-estimates cluster within a tight region and nearly all of the confidence regions overlap. While the theoretical backazimuth of 322.1°(line) is within the spread of observed azimuths for Nevada (distance 83°) of 318° to 322°, the predicted horizontal slowness $p_{\|} = \sqrt{{p_x}^2 + {p_y}^2}$ of 5.13 s/° is not located within the range of observed values of 4.41 to 4.86 s/°. Table 4 gives average azimuth and slowness for the Nevada events as 320.8°±1.8°and 4.56s/°±0.21s/°. Compared with predicted values this suggests a significant deviation in slowness, but not in azimuth.

TABLE 4: Significance of Azimuthal and Slowness Deviations

Source Region	Predicted θ	Observed θ_{obs}	Predicted $p_{\|}$	Observed $p_{\|_{obs}}$	$\frac{\|\theta-\theta_{obs}\|}{\sigma_\theta}^*$	$\frac{\|p_{\|}-p_{\|_{obs}}\|}{\sigma_{p_{\|}}}^*$
Nevada	322.1°	320.8°± 1.8°	5.13s/°	4.56s/°± 0.21s/°	0.7	**2.7**
Tuamotu	310.7°	320.9°± 3.0°	3.13s/°	3.04s/°± 0.26s/°	**3.4**	0.3
Poland	31.7°	28.5°± 2.1°	13.75s/°	12.75s/°± 0.50s/°	**1.5**	**2.0**

* Significant deviations of azimuth and slowness (larger than one σ) are shown in bold-face.

For the Tuamotu Archipelago events, backazimuths are in the interval 316° to 326° and deviate clearly from the predicted backazimuth of 311°. Table 4 shows that this azimuthal deviation is significant, while the slowness deviations is not. For the teleseismic events, standard deviations computed from observed values are in fact somewhat smaller than their formal uncertainties would suggest.

Figure 3-4b shows the results from inversion for (t_0, p_x, p_y), which effectively ignores topography across the array. The standard deviations are larger, but the two regions can still be easily distinguished. Compared with figure 3-4a the deviations from predicted values are larger indicating that ignoring topography across the array would in this case enhance the deviations. If we truncate the full inversion at three singular values we obtain figure 3-4c, which is essentially the same as in b. This is expected since the above discussion (table 2) showed that the smallest singular value, which is omitted here, controls almost exclusively the contribution of p_z.

Figure 3-4a shows that array mislocation effects still exist if we take topography into account particularly for the South Pacific. Table 4 suggest that the Nevada events experience significant slowness deviation, while the Tuamotu events experience significant azimuthal deviation. This indicates that the deviations are not caused by systematic biases of the inversion procedure. In fact for the events in this paper the full SVD solution is virtually indistinguishable to the least-squares solution indicating that we are dealing with a purely overdetermined problem. Hence, p_z is resolved and model biases from damping are not important in this case.

Now we test consistency of (p_x, p_y)-estimates for regional data. Events 12 to 18 in table 3 are a set of regional events from Poland, all of which are mining-induced events from the same source area (Rudno). Error bars of individual slowness components vary between 0.2 to 0.6 s/°, comparable to ones for teleseismic events. Figures 3-4d, e and f show horizontal slownesses p_x and p_y similar to figure 3-4a, b and c. Estimates in figure 3-4d again deviate from the predicted value shown by the end of the line. The azimuthal range is 26° to 31°, while the predicted azimuth is 31.7°. All inversion types give smaller horizontal slowness $p_{\|}$ than predicted (13.75 s/°), an effect which has previously been observed by Schweitzer (pers.comm.). Table 4 shows that both azimuthal and slowness deviations are significant. The scatter of azimuths and slownesses from Table 4 is comparable to formal errors of individual events. The different estimates are consistent suggesting that the error procedure is not only internally consistent, but gives us appropriate formal errors for the use in interpretations. There is one outlier with large error bar (event 14). Since it appears in all inversions, it is not a feature of the inversion method, but of the data set. Such large apparent uncertainty is suspect if sufficient care was taken in determining the travel times. They may be caused by timing errors in this early stage of the deployment. Standard errors, in fact, are an excellent tool for quality control of the data. Slownesses $p_{\|}$ and azimuthal deviations for the full inversion are not apparent in the reduced inversions.

If topography causes the difference in azimuth between figures 3-4a and b and 4d and e respectively, we can test this by predicting the pattern for synthetic data. For a set of events spaced at intervals of 10°and 1 s/°, figure 3-5 gives the predicted effect of ignored topography on p_x and p_y in the teleseismic slowness window of figure 3-4a. The maximum effect at steep

incidence is a shift of about 0.6 s/° eastwards (106°), which has been apparent in figure 3-4 as the main difference between the inversions accounting for and ignoring topography. The elevations in figure 3-1 show that most stations in the Southeast are more than 150 meters below the reference station C2, while a number of central and northwestern stations are above -60 meters. This asymetry in topography induces the observed regular pattern of figure 3-5. The arrows are essentially perpendicular to the direction of the topographic ridge on figure 3-1, since topography barely varies in that direction. The eastward direction of the arrows can be understood as an effect of the East-to-West asymetry of station distribution with respect to elevation. Ignoring topography, an average plane wavefront fit to the travel times therefore is tilted to the West causing the artificial Eastern component of the horizontal slowness components. The regularity of the pattern results from averaging over the whole array for each event. However, the effect is not constant for all azimuths and slownesses. For larger slowness the effect decreases and scatters in azimuth.

Left-over deviations in azimuth and slowness given in table 4 are true effects of lateral heterogeneity.

We have seen in the discussion of the inversion that it is important to suppress systematic errors from topography. Other potentially systematic effects are estimated to be small: The influence of Earth ellipticity should be an order smaller than our model errors. For a small array, wavefront curvature is negligible for epicentral distances larger than 100 km. Delays in the weathering layer are so far not accounted for, but residuals after the reduced inversion for (t_0, p_x, p_y) show a clear correlation with elevation confirming the local velocity estimate of 5.2 km/sec. It is clear that corresponding error vectors for S phases would be even larger, by a factor of v_P/v_S.

3.4 Results

Measurement errors of individual horizontal slowness components p_x and p_y from regional and teleseismic GERESS data vary in this study between 0.2 and 0.6 s/°. Data producing larger errors, are considered as suspect. Average azimuthal uncertainties (formal errors) are about 5° for teleseismic data, but about 2° for regional data despite reduced signal coherence. The observed scatter of $p_{||}$ and θ values for regional events from Poland is similar to formal errors, while teleseismic events scatter somewhat less than expected from formal errors.

We established that array mislocation effects from several source regions are significant. The strongest effect occurs for Tuamotu events, with backazimuths deviating by about 10° to more Northern angles and slownesses from Nevada, which deviate by about 0.5 s/° to smaller values. Both azimuths and slownesses from Poland deviate significantly: (4° to more northern backazimuths) and about 1.0 s/° to smaller values.

Although paths under the receivers are similar for events from Nevada and Tuamotu, they are perturbed differently: Significant effects are found for the teleseismic events as slowness deviations for Nevada, but azimuthal deviations for Tuamotu. Such a different behaviour is difficult to explain by lateral heterogeneity under the receivers alone. Distant heterogeneity is apparently involved.

Elevation changes of more than 100 meters across the array give rise to effects of the same order and must be taken into account for small arrays to avoid systematic errors. Ignoring topography or correspondingly the vertical slowness introduces artificial array mislocation effects for all three regions, which for GERESS amounts to a shift in approximately Eastern direction of up to 0.6 s/°, which is on the same order of measurement uncertainty. With elevation changes, GERESS acts as a 3D array. It supplies a direct estimate for the local velocity under the array, which for GERESS is 5.2 km/sec.

Significant leftover slowness and azimuthal deviations apparently result from lateral heterogeneity somewhere along the ray paths. The prime candidate is heterogeneity under the receiver region, but influences from heterogeneity along the path or in the source region are apparently also involved. This will be studied more closely in the future. Lateral heterogeneities are also a major cause of the discrepancy between the size of our measurement error and the error inferred from source mislocation studies which is larger by a factor of three to ten.

The GERESS data set may serve as a basis for classifying mislocations in the whole azimuth-slowness domain in order to improve source location procedures. Another major interest of subsequent studies is to use those data as constraints in determining the 3D structure of Earth.

References

Berteussen, K.A. (1975). Array analysis of lateral inhomogeneities in the deep mantle, *Earth and Planetary Science Letters* 28, 212-216.

Bokelmann, G.H.R. (1992). Upper and lower mantle small-scale heterogeneity studied by systematic analysis of portable broadband waveforms and traveltimes, PhD Thesis, Princeton University, Princeton, NJ, USA.

Bokelmann, G.H.R. (1993). Array Tomography for Body Waves: Inversion of Travel Times and Ray Parameters, *Annales Geophysicae*, Part I, p. C-47.

Burdick, L.J., Powell, C. (1980). Apparent velocity measurements for the lower mantle from a wide aperture array, *Journal of Geophysical Research* 85, B7, 3845-3856.

Chinnery, M.A., Toksöz, M.N. (1967). P wave velocities in the mantle below 700 km, *Bulletin of the Seismological Society of America*, 57, 199.

Davies, D., Sheppard, R.M. (1973). Evidence for lateral heterogeneity in the Earth's mantle, *Nature* 239, 318-322.

Faber, S., Plomerová, J., Babuska, V. (1986). Deep-seated lateral velocity variations beneath the GRF array inferred from mislocation patterns and P residuals, *Journal of Geophysics* 60, 139-148.

Fyen, J. (1987). Improvements and modifications, Semiannual Technical Summary, 1 October 1986-31 March 1987, NORSAR Sci. Rep. 2-86/87, Kjeller, Norway.

Gjoystdal, H., Husebye, .E.S., Rieber-Mohn, D. (1973). One-array and two-array location capabilities, *Bulletin of the Seismological Society of America*, 63, 549.

GSE/35/CRP/228 (1993), Seismological Evaluation of the Group of Scientific Experts' Second Technical Test (GSETT-2).

Harjes, H.P. (1990), Design and siting of a new regional array in central Europe, *Bulletin of the Seismological Society of America* 80, B, 1801-1817.

Harjes, H.P., Jost, M.L., Schweitzer, J., Gestermann, N. (1993). Automatic seismogram analysis at GERESS, *Computers&Geosciences*, 1, 2, 157-166

Hu, G., Menke, W. (1992). Formal inversion of laterally heterogeneous structure from P-wave polarization data, *Geophysical Journal International* 110, 63-69.

Johnson, L.R., (1969). Array measurements of P velocities in the lower mantle, *Bulletin of the Seismological Society of America*, 59, 973-1008.

Krüger, F., Weber, M. (1992), The effect of low-velocity sediments on the mislocation vectors of the GRF array, *Geophysical Journal International* 108, 387-393.

Okal, E., Kuster, G. (1975), A teleseismic array study in French Polynesia; Implications for distant and local structure, *Geophysical Research Letters* 2, 1, 5-8.

Walck, M.C., Minster, J.B. (1982). Relative array analysis of upper mantle lateral velocity variations in Southern California, *Journal of Geophysical Research*, 87, B5, 1757-1772.

Weichert, D.H. (1972). Anomalous azimuths of P: Evidence for lateral variations in the deep mantle, *Earth and Planetary Science Letters* 17, 181-188.

Weichert, D.H. (1975). The role of medium aperture arrays: The Yellowknife system, in: *Exploitation of Seismograph Networks*, ed. by K.G. Beauchamp, Nordhoff International , Leiden.

Wright, C. (1981), Comments on 'Apparent Velocity Measurements for the lower mantle from a wide aperture array' by L.J. Burdick and C. Powell, *Journal of Geophysical Research*, 86, B12, 11927-11930.

FIG. 3-1: a) Array locations of the GERESS array in Southeastern Germany in meters (Gauss-Krüger coord.). Filled circles show the 25 vertical shortperiod instruments used in this paper. Triangles and rectangles give locations of added 3-component instruments. Both horizontal distances and elevations (labels) are in meters. Topographic variation across the array of about 200 meters is shown by contour lines (increment of 25 meters), while the number after the station name gives instrument elevation (located in vaults) relative to 1000 meters, the first solid contour.

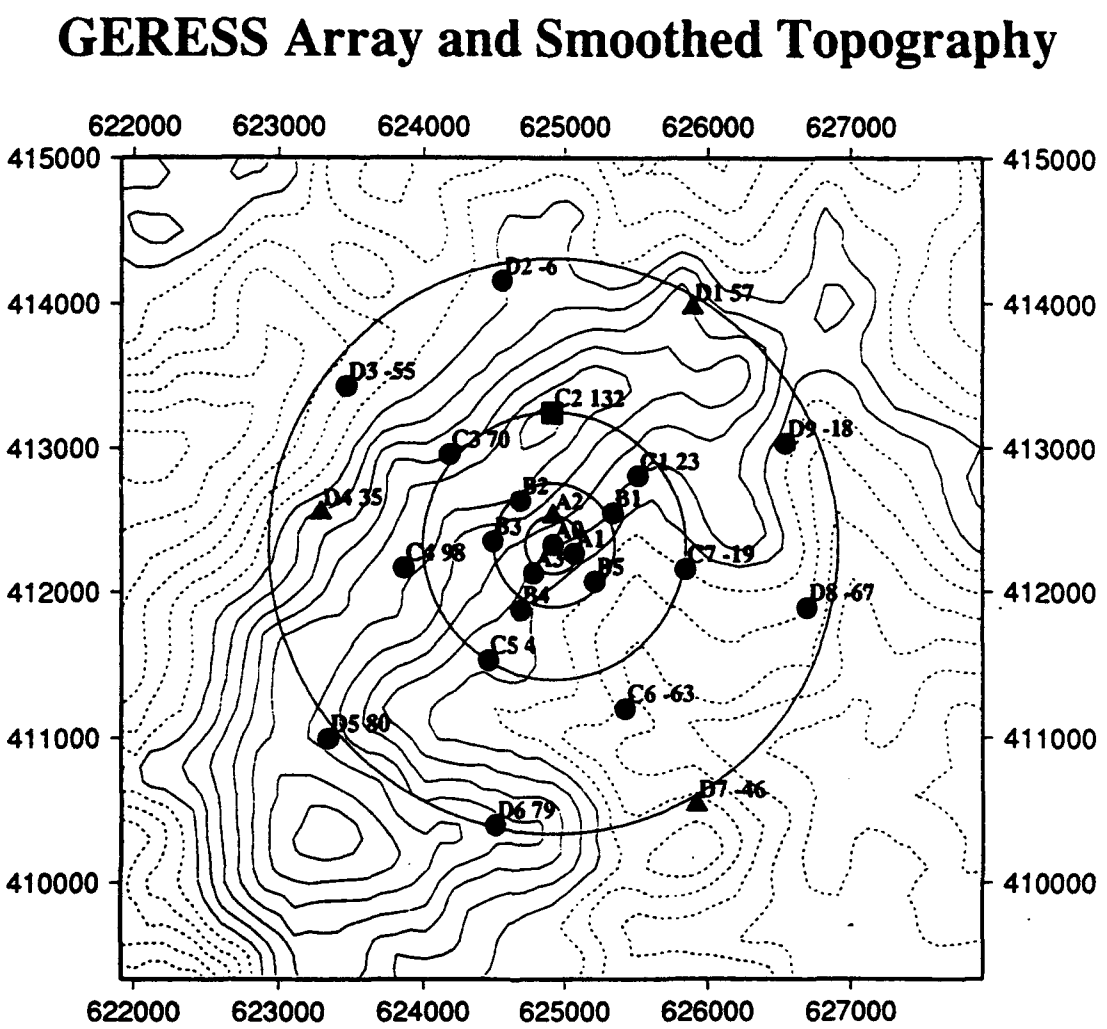

FIG. 3-2: Histogram of local velocity estimates $c = \frac{1}{\sqrt{p_x^2+p_y^2+p_z^2}}$ from the regional and teleseismic events in table 3. The mean value is 5.2 km/second.

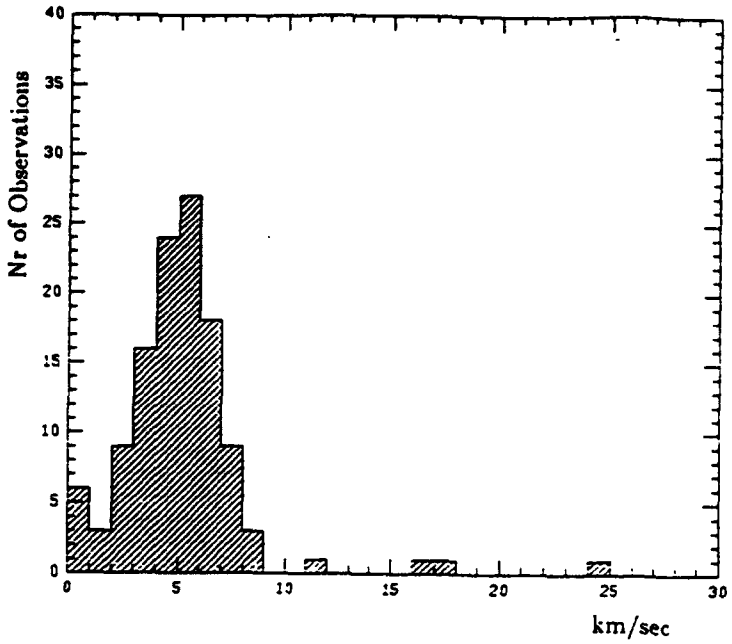

FIG. 3-3: Waveform data from a French nuclear test on Fangataufa, Tuamotu, South Pacific (event 6 in table 1; bandpass at 0.1 and 2.5 Hz). Note the strong coherence of the PKP phase, particularly within the first two seconds of the waveform. This coherence allows determination of a relative time lag with high accuracy.

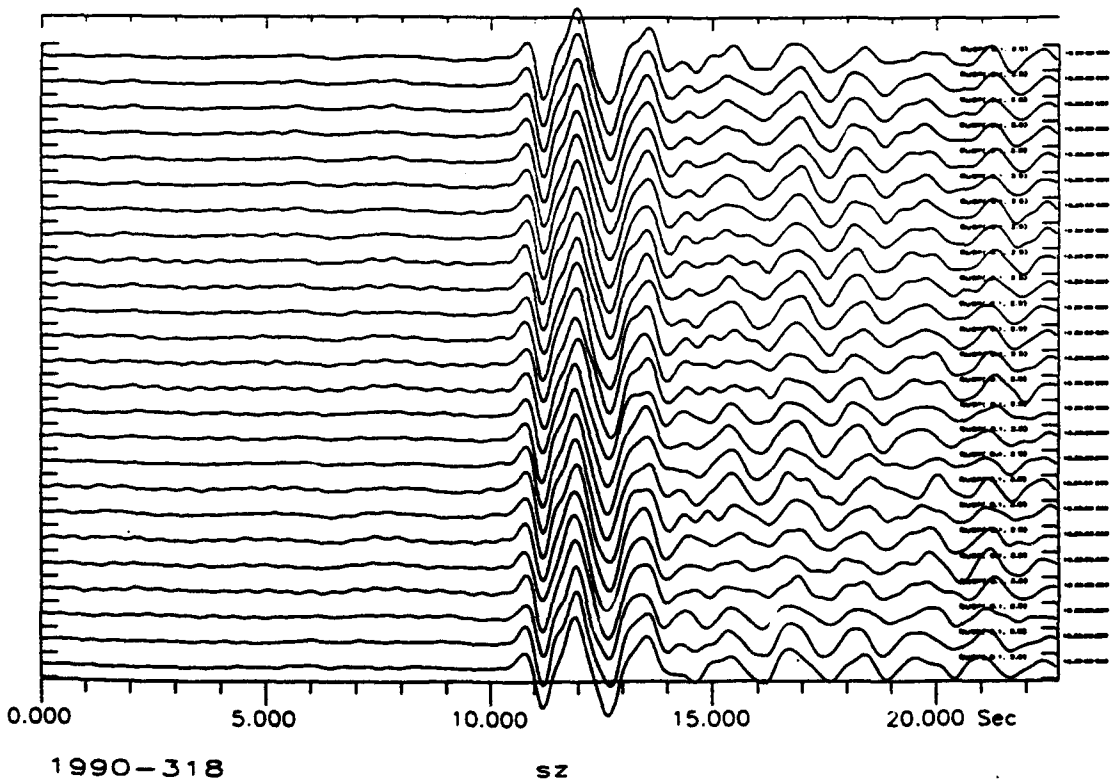

FIG. 3-4: a) Horizontal slownesses (p_x, p_y) in s/° for the teleseismic events 1 to 11 in table 3, where we solve for (t_0, p_x, p_y, p_z). Nevada and Southern Pacific events form disjoint sets with standard errors of 0.2 to 0.6 s/°. For the South Pacific there is a clear azimuthal offset from the predicted value of about 9°. b) same as in a, but we solve for (t_0, p_x, p_y) ignoring topography. Errors are larger and the two regions are not as well-separated; c) same as in a, but restricting the inversion to 3 singular values. This inversion gives essentially the same result as b, since the omitted fourth singular value almost completely described p_z. Note that results for b and c (ignoring topography) deviate more strongly from the predicted values than a). d), e) and f) give corresponding results for regional events 12-18 from a Polish mining area. Note that after accounting for array topography the average of the estimates deviates from predicted value in azimuth but particularly in slowness.

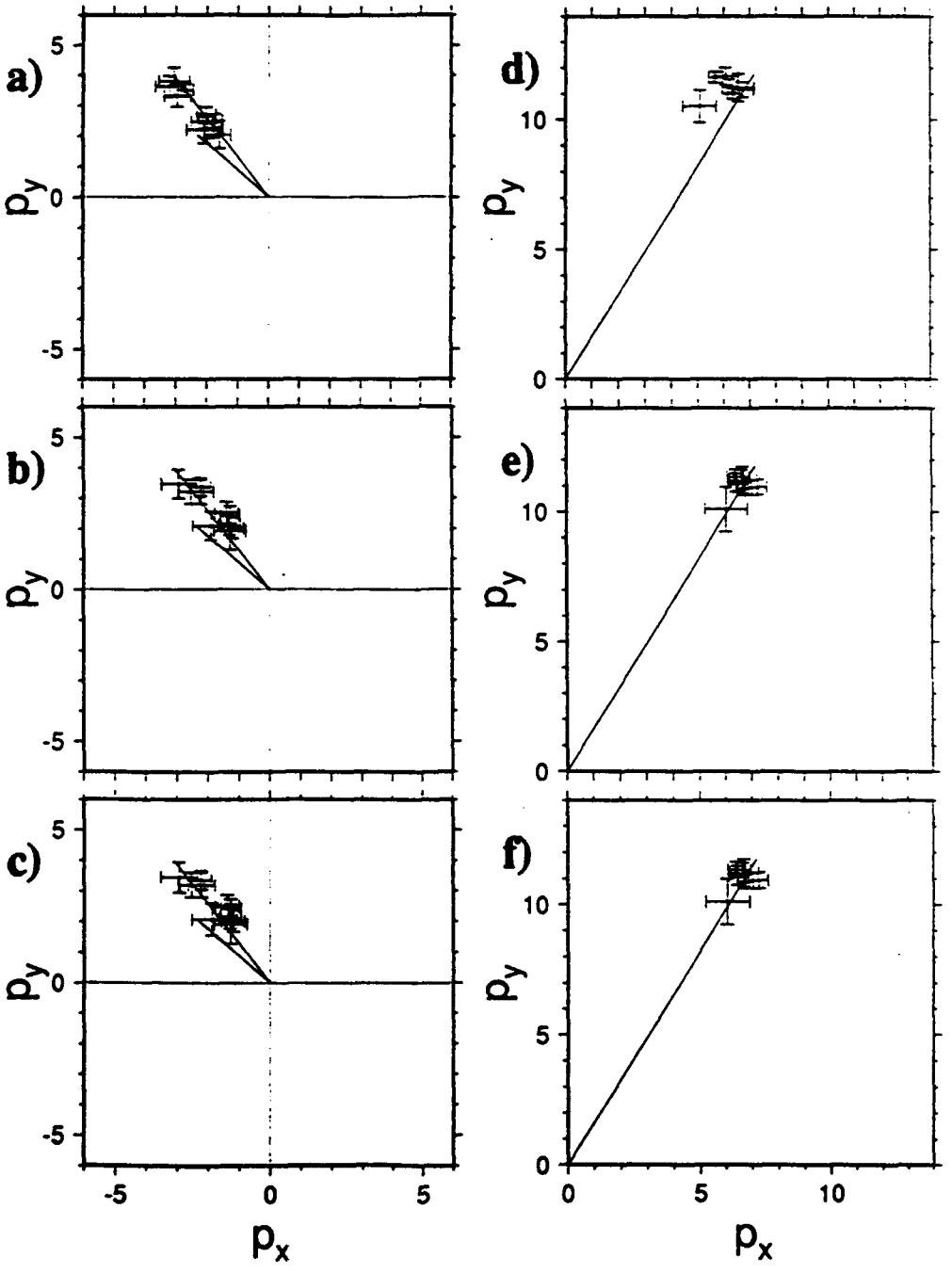

FIG. 3-5: The effect of GERESS topography on the slowness vector of teleseismic events is an eastward shift ($\Delta\theta \approx 106°$) of up to 0.6 s/°, almost independent of the source location. For larger slowness the effect decreases and angles of the shift scatter.